Universidade de Aveiro Departamento de química
Ano 2020

Ana Lia Guimarães Lourenço da Fonseca

Desenvolvimento de uma nova biotinta baseada em interações supramoleculares hospedeiro-convidado

Development of a novel bioink based on host-guest supramolecular interactions

2020

Universidade de Aveiro Departamento de química
Ano 2020

Ana Lia Guimarães Lourenço da Fonseca

Desenvolvimento de uma nova biotinta baseada em interações supramoleculares hospedeiro-convidado

Development of a novel bioink based on host-guest supramolecular interactions

Dissertação apresentada à Universidade de Aveiro para cumprimento dos requisitos necessários à obtenção do grau de Mestre em biotecnologia, realizada sob a orientação científica da Doutora Susanna Piluso, Pós-doutorada no Departamento de Medicina Regenerativa da Centro Médico Universitário de Utrecht e do Professor Doutor João Mano, Professor Catedrático de Química do Departamento de Química da Universidade de Aveiro

o júri

presidente	Prof. Doutor Ana Maria Rebelo Barreto Xavier professora auxiliar da Universidade de Aveiro
arguente principal	Doutor Vítor Manuel Abreu Gaspar investigador doutorado (nível 1) da Universidade de Aveiro
orientador	Prof. Doutor João Filipe Colardelle da Luz Mano professor catedrático da Universidade do Porto

agradecimentos

Em primeiro lugar, gostaria de dar um agradecimento especial à Dr. Susanna Piluso por me ter dado esta oportunidade, por me ter orientado e por estar sempre disposta a partilhar o seu conhecimento comigo. Foi um prazer conhecê-la. Gostaria também de agradecer ao Prof. Dr. João Mano por ter criado a ligação entre a Universidade de Aveiro e o Centro Médico Universitário de Utrecht sem a qual esta tese não teria acontecido. Muito obrigada ao Prof. Dr. Jos Malda, por me ter aceite no seu grupo e por produzir ciência de excelência. Obrigada ao Centro Médico Universitário de Utrecht por todo o apoio e recursos que deixa à disposição dos seus funcionários e alunos. Obrigada ao programa ERASMUS+ que me concedeu uma bolsa de estudo que ajudou a aliviar os meus encargos económicos durante este projeto. Obrigada a toda a equipa pelo espirito de entreajuda e bom ambiente de trabalho. Obrigada aos alunos de douturamento que se disponibilizaram para fazer reuniões mensais para ajudar todos os alunos com os seus respetivos estágios e por toda a ajuda com o trabalho laboratorial. Por fim, gostava de agradecer à minha família. À minha mãe pelo apoio incondicional. Ao Pieter por todos os conselhos. Aos meus avós por todo o amor incondicional. Ao meu tio que está sempre pronto a defender-me. À Juliana, a minha irmã mais velha que me acompanha desde sempre. Amo-vos!

acknowledgements

First and foremost, I would like to give a special thanks to Dr. Susanna Piluso, for giving me this opportunity, for having me as a student and for always being willing to share her knowledge. It was a pleasure meeting you. Many thanks to Prof. Dr. João Mano for bridging University Medical Center Utrecht and Aveiro University which made possible this thesis. Thank you, Prof. Dr. Jos Malda, for allowing me to work in your lab, and for doing great science. Thank you to the University Medical Center Utrecht for all the resources and support that provides to its employees and students.Thank you to ERASMUS+ program that appointed me with a scholarship that helped to aliviate my additional ecomic expenses during this project.Thanks to all students working in the lab for always being willing to lend a helping hand and for the friendly working environment. Many thanks to the phD students, for the monthly meetings and for your help with the lab work. Many thanks to my family. To my Mom for being my rock, I would not be here if it was not for you. To Pieter for all you support and for your out of the box advice. To my Grandparents for your unconditional love. To my Uncle, for always having my back. To Juliana, my big sister who has always been there. I love you!

palavras-chave

Hidrogéis; Biotinta; Interações supramoleculares hospedeiro-convidado; Seda; Gelatina

resumo

Atualmente, devido à escassez de tecidos e órgãos para transplante há uma crescente atenção dada à área da medicina regenerativa. As técnicas de bioimpressão 3D são usadas para criar células encapsuladas em estruturas tridimensionais que mimetizam a rede sólida 3D que a maioria das células necessita para sobreviver. Os hidrogéis, são candidatos ideais para formar estas estruturas porque possuem um elevado nível de hidratação e elasticidade semelhante à dos tecidos nativos. No entanto, as biotintas utilizadas na bioimpressão 3D necessitam de ser, simultaneamente, biocompatíveis e imprimíveis, o que torna a sua formulação desafiante. Por esta razão, ainda há espaço para melhorar os biomaterials que existem atualmente para cumprir esta função.

Com o intuito de ultrapassar este desafio, a preparação de um biotinta feita de seda e de gelatina modificada com ciclodextrina (GelM) foi investigada. Enquanto a seda possui boas características mecânicas e elasticidade a gelatina oferece motivos de bioadesão.

Os resultados mostram que as interações hospedeiro-convidado entre a ciclodextrina presente na gelatina e as tirosinas da seda aumentam a viscosidade da mistura Seda - GelM em repouso e fazem com que esta diminua a sua viscosidade quando uma força lhe é aplicada.

Para além disso, a presença destas interações físicas parece estar correlacionada com a capacidade de autorregeneração e com o aumento da elasticidade da estrutura. Todas estas caraterísticas são vantajosas para a impressão e viabilidade celular.

Adicionalmente, os testes preliminares de impressão sugerem que a formulação desenvolvida pode ser impressa.

keywords Hydrogel; Bioink; Host-guest supramolecular interactions; Silk; Gelatine

abstract

At present, due to the shortage of tissues and organs for transplantation, there is a growing attention towards the field of regenerative medicine. 3D bioprinting techniques are used to create cell embedded scaffolds that mimic the solid 3D network that most cells require to survive. Hydrogels are ideal scaffold candidates because of their hight water content and tissue-like elasticity. However, bioinks used in 3D bioprinting need to be simultaneously fine-tuned to be biocompatible and printable, as such, there is still a need for improvement.
To tackle this challenge the preparation of a bioink made of silk and cyclodextrin modified gelatine (GelM) was investigated. While, silk provides strong mechanical features, elasticity and controllable biodegradability, gelatine offers bio-adhesive motifs. The results show that the host-guest interactions between the cyclodextrin on gelatine and the Tyr on silk polymeric chain seemed to be correlated with shear-thinning behaviour and an increase in viscosity of the Silk-GelM blend at rest.
Furthermore, the presence of these physical interactions imparted self-healing properties and caused an overall increase in elasticity of the construct. All these characteristics are advantageous for printability and cellular viability. Additionally, preliminary printability tests strongly suggest that the developed formulation can be successfully printed.

Table of Contents

Abbreviation Index

3D – three dimensional

AM – addictive manufacturing

BF – basic fuchsin

Borax – sodium tetraborate tetrahydrate

$Ca(NO_3)_2$ – calcium nitrate

$CaCl_2$ – calcium chloride

CAD – computer-aided design

CD – cyclodextrin

DMF – dimethylformamide

DM_{TNBS} – degree of modification measured using the TNBS assay

EB – extrusion based bioprinting

ECM – extracellular matrix

EDC – 1-ethyl-3-(-3-dimethylaminopropyl) carbodiimide

G' – storage modulus

G'' – loss modulus

Gel – unmodified gelatine

GelM –modified gelatine

HA – hyaluronic acid

HCl – hydrochloric acid

kDa – kilo Dalton

LiBr – lithium bromide

LIFT – laser-induced forward transfer

LiSCN – lithium thiocyanate

LVR – linear viscosity region

MW – molecular weight

Na_2SO_3 – sodium carbonate

NHS – N-hydroxysuccinimide

PBS – phosphate-buffered saline

PEG – polyethylene glycol

PEI – polyethylenimine

PNIPAm – poly (N-isopropylacrylamide)

PVA – poly (vinyl alcohol)

RBFM – riboflavin 5’-monophosphate sodium salt hydrate

RET – rubber elastic theory

SDS – sodium dodecyl sulphate

SPS – sodium persulfate

STL – stereolithography;

S-β-CD – succinyl-β-cyclodextrin

TNBS – 2,4,6-trinitrobenzenesulfonic acid or picrylsulfonic acid

Tyr – tyrosine residue

β-CD – β-cyclodextrin

List of Figures

List of Tables

Introduction

A. Regenerative medicine

Regenerative medicine is a field of research that focuses on replacing or regenerating tissues or organs in order to establish their normal function[1]. This can be achieved with several strategies[2], one of them being the creation of functional constructs made of: cells; growth factors, and a scaffold to support the restoration of the structure and functionality of the damaged tissue or organ[3,4].

Scaffolds are used to mimic extracellular matrix (ECM) characteristics and function, since most cells, apart from blood cells, require a solid matrix called ECM to attach to[4]. Thus, a scaffold provides mechanical support while the newly formed tissue matures, and it can also, concurrently, provide these damaged or degenerated tissues or organs with cells and/or growth factors that aid in restoration[3].

B. Hydrogels

Hydrogels are three-dimensional (3D) networks made of crosslinked hydrophilic polymer chains[5]. Due to their hight water content, tissue-like elasticity and ease of diffusion of nutrients and waste, hydrogels are ideal candidates to mimic the ECM[6–9]. They can be naturally and synthetically derived[10].

B.1 Naturally derived hydrogels

Naturally derived hydrogels are created from a variety of natural sources of polymers using several cross-linking methods (e.g. physical, covalent, ionic)[9,10]. Silk[11], gelatine[12,13], fibrin[14], collagen[15], chitosan[16], hyaluronate[17,18], agarose[19] and alginate[16] are some examples of natural polymers used to prepare hydrogels.

Most naturally derived hydrogels show inherent bioactivity, biocompatibility and biodegradability[9,20]. Polymers derived from vertebrates (e.g. gelatine, collagen and fibrin) have inherent signalling molecules for cell adhesion, however, polymers derived from other organisms such as algae and seaweed lack such signalling molecules (e.g. alginate[21] and agarose[22])[14].

These chemical cues (e.g. bioactive molecules for cell adhesion and migration), although not mandatory for cell viability, can promote cellular proliferation[3,9,23].

Furthermore, the biodegradation rate can influence to some extent the formation of specific neo-tissues[24]. Khetan and co-workers showed that the high/low biodegradability

of hyaluronic acid (HA) hydrogels with equivalent matrix mechanics directed stem cell fate to the osteogenic/adipogenic pathway, respectivelly[25].

Natural hydrogels normally have weak mechanical properties and low reproducibility due to high batch-to-batch variation[3,20]. Additionally, some cell types (*e.g.* stem cells) can be sensitive to these variations which might make it difficult to evaluate cellular behaviour in naturally derived hydrogels[3,20].

B.1.1 Silk

Silk fibroin is a natural protein biopolymer that has a long history of use in biomedical applications. Mild adverse reactions were observed when using silk, however there are strong indications that sericin was the cause of the adverse reactions[26–28]. Thus, there is a widespread acceptance that properly degummed and sterilized silk derived biomaterials have good biocompatibility. Nowadays, silk fibroin, is used for sutures in lips, eyes, oral surgeries and in skin wounds[27,29]

Silk can be obtained from arthropods (*i.e.* silkworms, spiders, scorpions, mites and bees) that possess silk producing glands that generate silk proteins to be spun into fibers during metamorphosis[30]. One of the most investigated silks thus far is the silkworm silk[31].

There are two types of silkworm silk: the mulberry silk and the non-mulberry silk produced by silkworms of the *Bombynacidae* and the *Saturniidae* family, respectively. *Bombyx mori* mulberry silk (**Figure 1-A**) is the most widely studied [32]. It is extremely convenient for genetic engineering because it is easily available[32], and its entire DNA sequence is known[33,34].

Raw silk, spun by silkworm silk grands, is made of two parallel fibroin fibers coated with sericin. Sericin is a gum-like protein responsible for raw silk's adhesive nature[35], it is mainly made of serine (32%)[35] (**Figure 1-B**).

Mulberry silk fibroin produced by *B. mori* is a fibrous glycoprotein comprised of two polypeptide chains connected by a disulphide bond, namely: heavy (H) (~350 kDa) and light (L) (~26 kDa) chain.

A glycoprotein (P25) (~30 kDa) is non-covalently connected to the H-L complex. P25 plays and important role in maintaining the integrity of the complex, the ratio H-chain: L-chain: P25 is of 6:6:1[36].

This structure is called the fibroin elementary unit, which allows for the solubility and transportation of large amounts of fibroin through the silkworm's silk gland before being spun into fibers[36].

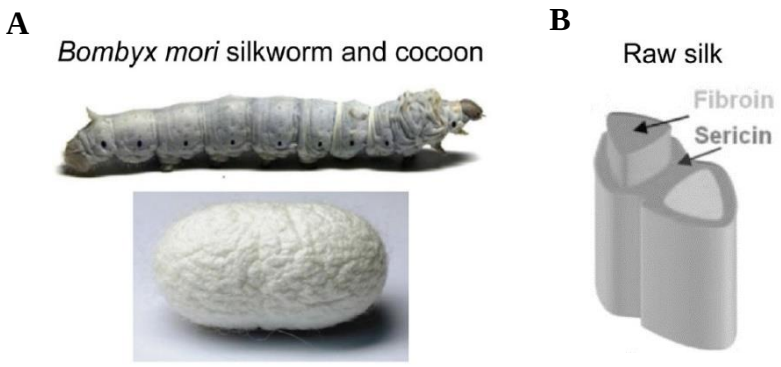

*Figure 1 – **A.** Bombyx mori silkworm and cocoon; **B.** Raw silk comprised of two fibroin strands coated with sericin. Figure adapted from Koh et al[36].*

The H chain consists of hydrophobic domains with Gly-X (X = Ala; Ser; Tyr; Thr or Val) repeats, that can form β-sheets interspaced by hydrophilic domains that contain non-repetitive sequences[34] (**Figure 2 - A**). The most abundant amino acids of the H chain are glycine (43-46%); alanine (25-30%); serine (12%) and tyrosine (5%)[33,34,37].The L chain is hydrophilic, quite elastic and plays little mechanical role due to its relatively small size[38,39] (**Figure 2 - B**).

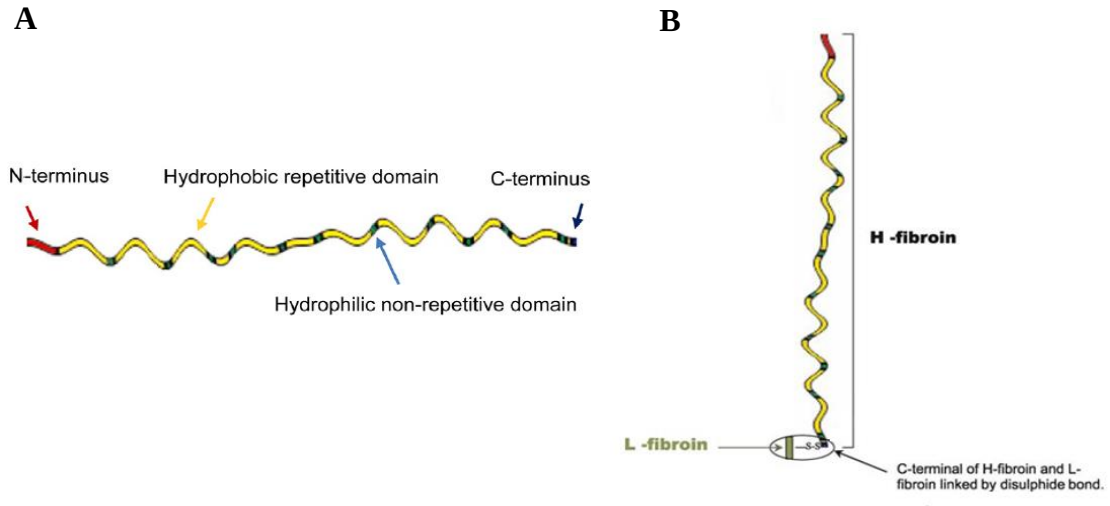

*Figure 2 – **A.** Heavy chain of silk fibroin with 12 hydrophobic interspaced by 11 hydrophilic domains. **B.** Schematic representation of the L-fibroin chain and the H-chain connected by a disulphide bond. It is evident form this representation the difference in size of the two chains Figure adapted from Koh et al[36] and Foo et al[39], respectively.*

Silk secondary structure encompasses nanocrystals (β-sheets) formed by the repeated amino acid sequences of the hydrophobic domains in silk polymeric chains and random coils comprised by the bulky and polar side chains of the hydrophilic domains that form the amorphous part of the structure (**Figure 3**)[40–42].

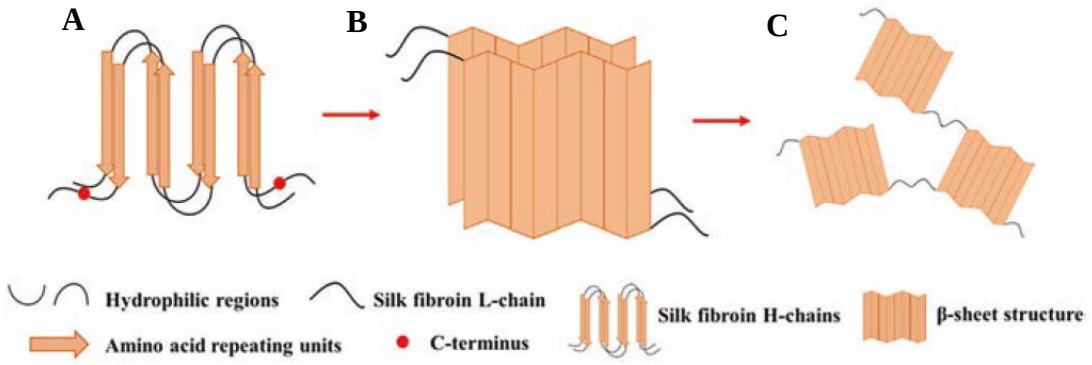

Figure 3 - Schematic representation of the formation of β-sheet and random coils by silk fibroin. ***A.*** *Formation of the H-L complex;* ***B.*** *β-sheet formation by the H-chains;* ***C.*** *The β-sheets structures are connected by the amorphous domains. Figure adapted from Oliveira et al[42].*

Many types of silk, including *B. mori* silk fibroin are polymorphic because their high glycine content allows for great conformation variability[43]. Polymorphism is a characteristic of materials that have the ability to crystalize with two or more distinct molecular arrangements[44].

Silk fibroin polymorphs are silk I – the silk fibroin conformation on the silkworm gland prior to crystallization (random coils and α-helix)[45,46]; silk II – the silk fibroin conformation after being spun (has a β-sheet secondary structure)[47] and silk III – the assembly of silk fibroin in the interface air/water[48].

Silkworm silk nanocrystals or crystalline domains arrange themselves into microfilament bundles (0.5-2 μm diameter)[49,50] (**Figure 4**). All silkworm silk types have similar hierarchical structural arrangements despite differences in their primary organization and secondary structure at the nanometer scale[38].

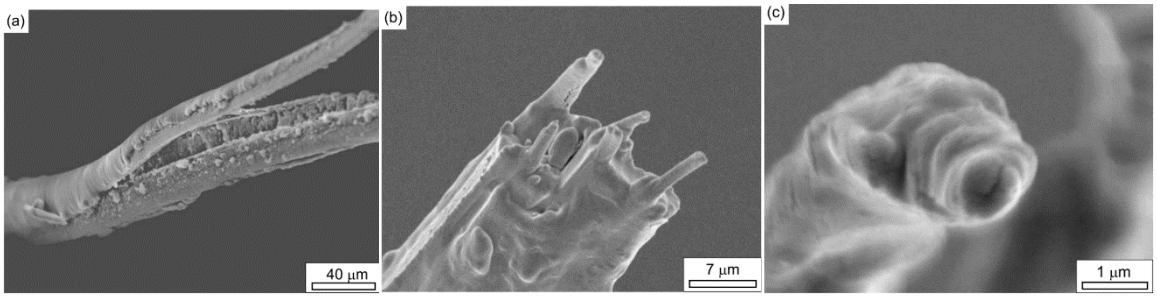

Figure 4 – ***a)*** *Silk fiber split into several microfibers;* ***b)*** *detail of one of the microfibers with microfilaments bundles projecting from it and* ***c)*** *surface fracture of a microfilament bundle. Figure adapted from Poza et al[50].*

Silk can be used as a biomaterial as native silk fibers or as a regenerated material from a silk solution, for both approaches it is necessary to remove sericin[38].

To obtain a silk regenerated material, silk needs to be solubilized. Mild manufacturing conditions such as room temperature, neutral pH and no shear force application can be used in addition to water to prepare silk-based systems[38]. Because silk fibroin solubility in water is dependent on its secondary structure (soluble when in its α-helix and random coil and insoluble when in the β-sheets conformation), to solubilize silk, the hydrogen bonds and hydrophobic interaction responsible for regulating the intra- and inter-bond interactions need to be disrupted[51]. To this end concentrated solutions of chaotropic salts (*i.e.* LiBr[27]; $CaCl_2$/ethanol/water[52]; LiSCN[53]) or ionic liquids[54] are used to dissolve mulberry silk. Silk can remain soluble for days and weeks depending on its storage temperature, pH and silk concentration[55].

To turn silk fibroin solution into a 3D form disruption of water hydration is required to confer silk fibroin with good resistance to dissolution and degradation (either enzymatic or thermal) by the induction of β-sheet conformation[31]. Processes like mechanical stretching[56] and ultrasonic treatments[57] can be applied in order to avoid the use of harsh chemicals[38].

Silk fibroin mechanical properties are tightly connected to its secondary structure and hierarchical organization, particularly the precise control of the size, number, distribution, orientation and spatial arrangement of the crystalline and non-crystalline domains[38,58]. While the non-crystalline, amorphous domains provide elasticity[40], the crystalline domains contribute to silk's mechanical properties[58].

Silk shows good toughness, strength and ductility; in fact, silk fibers are tougher than Kevlar a high performance synthetic fiber[59]. It also has a high strength-to-density ratio, which is ten times higher than steel due to its small density[60]. Additionally, silkworm silk shows high extensibility and strain hardening behaviour which is particularly important in materials that absorb energy[61]. Strain hardening means the application of a deforming force makes the material stronger and less ductile. Due to its mechanical characteristics, silk has been used to develop tissue scaffolds for load bearing tissue engineering[38].

Although native silk fibers have good mechanical properties for the most part silk materials developed from silk fibroin solutions are weak and brittle[62,63]. These disparities

are thought to be due to differences in silks secondary structure and hierarchical supra-molecular organization[64,65].

Furthermore, silk's degradation rate is also dependent on its secondary structure and hierarchical supramolecular organization and as such regenerated silk fibroin biomaterials tend to degrade much faster than natural fibers[66].

Studies have shown that silk is degraded *in vivo* and that its degradability is tightly interconnected with the host's immune system[67]. Furthermore, cells *in vitro* also seem to mediate degradation, which supports the possibility of matrix remodelling *in vivo* with synchronized silk proteolytic degradation and native extracellular matrix regeneration[68,69].

Silk degradation does not release acidic degradation by-products and maintain its mechanical properties for a long period of time, which is advantageous when slow degradation and load bearing capacity are necessary[38].

B.1.2 Gelatine

Gelatine is a protein-based polymer that is the result of the hydrolysis of the fibrous protein collagen. Collagen can be extracted from bones, skin, and the connective tissues from animals (*e.g.* pig, calf, and fish)[70]. There are several different types of collagen that were identified, a summary is shown in **Table 1**[71].

Table 1 – Description of some of the different types of collagen. Table obtained from Karim et al[71].

Type	Description
Type I	This type occurs widely, primarily in connective tissue such as skin, bone, and tendons.
Type II	This type of collagen occurs practically exclusively in cartilage tissue.
Type III	This type strongly dependent on age: very young skin can contain up to 50%, but in the course of time this is reduced to 5–10%.
Other types	The other types of collagen are present in very low amounts only and mostly organ-specific.

Depending on the type of collagen hydrolysis, acidic or basic process, gelatine can be of type A or B, respectively. For the same gel strength, the two types differ in viscosity, type A is less viscous than type B and in their isoelectric point of 7-9.4 for type A and 4.5-5.3 for type B[72]. The differences in their isoelectric point are due to the de-amidation of the asparagine and glutamine residues which increases the corresponding acids (aspartic and glutamic acid, respectively)[73]. The de-amidation occurs in a greater extent in the basic hydrolysis[73].

Gel strength is defined using the Bloom test which determines the weight (in grams) that a specific plunger needs to have to depress the surface of a gel without breaking it. This test is run under specific conditions and the resultant gel strength is expressed as the Bloom value[70]. The gel strength is influenced by the amino acid composition, that is species specific and the molecular weight of the polymers[70].

Gelatine's amino-acid composition is very similar to collagen and is characterized by the Gly-X-Y sequence where X stands for proline and Y for hydroxyproline[71]. A typical amino acid composition of porcine skin gelatine is shown in **Table 2**.

As a result of being a degradation product of collagen, gelatine retains the Arg-Gly-Asp (*i.e.* RGD) motif, a cellular adhesion sequence, from its precursor. The RGD motif imparts gelatine with bioactive and bio-adhesive characteristics[74].

Collagen molecules are made of three α-chains (*i.e.* collagen triple-helix) that are intertwined and stabilized through hydrogen bonds. When it is denatured, the collagen chains totally or partially separate due to the destruction of the hydrogen bonds. After denaturation, the polymers exist in a coiled form[71].

Table 2 – Amico-acid composition of bovine skin gelatine (type B) and porcine skin gelatine (type A). Table adapted from Hafidz et al[161].

Amino acid	BSG (residues per 1000 total amino acid residues)	PSG (residues per 1000 total amino acid residues)
Nonpolar hydrophobic		
Alanine	33	80
Valine	10	26
Leucine	12	29
Isoleucine	7	12
Phenylalanine	10	27
Methionine	4	10
Proline	63	151
Total	139	335
Polar uncharged		
Glycine		
Serine	108	239
Threonine	15	35
Tyrosine	10	26
Total	2	7
	135	307
Polar acidic		
Aspartic acid	17	41
Glutamic acid	34	83
Total	51	124
Polar basic		
Lysine	11	27
Arginine	47	111
Histidine	Not detected	Not detected
Total	58	138

Industrial gelatine is a mixture of: α-chains (one polymer chain), β-chains (two α-chains covalently crosslinked) and ϒ-chains (three α-chains covalently crosslinked). The main difference between the α, β, ϒ chains, are their molecular weight α<β<ϒ[72].

Additionally, gelatine is thermosensitive, at low temperatures its strands self-associate creating a helical structure while as the temperature increases, they revert to a random coil conformation[75]. Thus, gelatine in gel form can be obtained at low temperatures (below 25-35°), due to its ability to form physical crosslinks, while above 35°C it easily liquefies[76,77].

As such, because gelatine's physical network tis broken apart at high temperatures gelatine hydrogels have poor mechanical strength and low shape fidelity and elasticity that limits their applications at the physiological temperature (37°C) [78,79]. To surpass this problem several strategies have been used such as: crosslinking the gelatine polymers[78,79] and mixing gelatine with another biomaterial with strong mechanical properties[80].

Gelatine possesses suitable biological properties that can support cell growth and function because it is biodegradable and biocompatible[74,81–84]. Additionally, because it is denatured, gelatine has low immunogenicity[84,85].

B.2 Synthetically derived hydrogels

Synthetic hydrogels, are created by reacting inert biomolecules, normally monomers and polymers, to form cross-linked networks[9]. Examples of synthetic polymers are polyethylene glycol (PEG), poly(vinyl alcohol) (PVA), poly(N-isopropylacrylamide) (PNIPAm) among others[9,10].

The general absence of signalling molecules, in these inert biomolecules, for cell adhesion and migration[86,87] results in low cell viability[3]. However, the addition of bioactive compounds such as peptide sequences[86,87] – that modulate cellular behaviour by providing binding sites - or growth factors[88] – that direct cellular differentiation - is a possible way to overcome the inert environment characteristic of the synthetic networks and regenerate a specific tissue.

A study by Zhang *et al.* showed that chondrocytes encapsulated in a PEG biodegradable hydrogels, with added degradation moieties, had enhanced cartilage tissue formation when comparing to its non-biodegradable counterpart[89].

These polymers show consistent and predictable properties because their chemical outlook is defined precisely by the selection of the network components[9]. As such, they are very attractive for studying the effects of specific biochemical and biophysical effects on cell function in comparison to natural hydrogels.

Moreover, synthetic hydrogels mechanical strength can be tuned[90]. Thus, they may be tailored to possess stronger mechanical properties[90] and deliver high shape fidelity constructs[3].

C . Crosslinking density

The crosslink density of a polymer network refers to the number of elastic active chains in a certain volume of material[9]. It impacts the water content of the hydrogel; the networks mesh size and the hydrogel mechanical properties[9]. Thus, influencing molecule diffusivity and material stiffness. The water content can be measured by the volumetric swelling ratio – the ratio of water-swollen gel volume to dry gel volume[9,91].

After being printed, a hydrogel construct will eventually collapse if not stabilized, because even a very viscous precursor solution will change its shape over time[3]. Hydrogels' mechanical properties can be controlled by changing the crosslink density of its network[10]. This is particularly useful for preserving a hydrogel printed construct structure by post-printing cross-linking.

Cross-linking can be physical (reversible interactions), chemical (irreversible interactions) or a combination of both[3].

C.1 Physical crosslinking

Physical crosslinking mechanisms are based on reversible, non-covalent interactions[92] which can be ionic/electrostatic interactions, hydrogen bonds, , hydrophobic/hydrophilic interactions, crystallization/stereocomplex formation (*e.g.* host-guest interactions), among others[93].

Physically crosslinked hydrogels show great compatibility with sensitive molecules (*e.g.* growth factors) and with living cells due to the absence of harmful chemical crosslinking agents and unreacted chemical crosslinkers[94]. Moreover, these non-covalent physical interactions between hydrophilic polymer chains may prevent the gel from dissolving immediately in an aqueous environment at a specific temperature[3].

C.1.1 Host-guest supramolecular interactions

The concept of supramolecular assembly refers to the "chemistry beyond the molecule"[95]. Because the non-covalent nature of the supramolecular bonds makes them weaker than covalent bonds, they can take part in thermodynamic or forcefully induced rearrangements that direct the assembly of molecules in a lengthy scale which exceeds, by far, that of single atoms or molecules[96]. This results in the formation of high order structures in biological proteins and tissues, it also permits the spontaneous and reversible binding of different molecular species[96]. This type of behaviour allows the development of dynamic and self-healing materials[97].

One subset of supramolecular chemistry are the host-guest interactions. These bonds are based on associations of a molecule that contains a cavity (*i.e.* a cavitand) with a suitable molecular guest[96]. For a host-guest interaction to occur the size of the host cavity needs to be complementary to the size of the guest molecule; they also need to have specific interactions (mainly through hydrophobic interactions)[98,99].

Host-guest molecular recognition can be used for the formation of supramolecular structures, for example: host-guest hydrogels[92]. Modifications, either as end groups or pendants, of polymers with guest and host molecules have been used to induce this host-guest structure assembly upon mixing (**Figure 5**)[96]. Rodell *et al.* has successfully created hydrogels based on host-guest supramolecular interactions by modifying HA polymer chains with adamantane (guest) and β-CD (host)[100]. While *Wang et al.* used the same approach but with PEG and polyethylenimine (PEI) as polymer precursors[101].

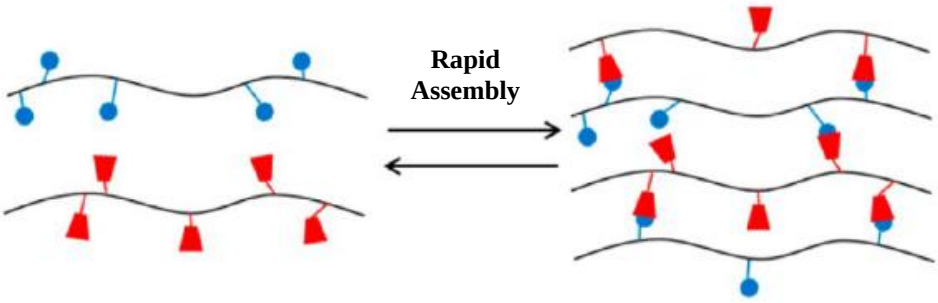

Figure 5 - Host-guest interaction (figure on the right) upon mixture of a pendant modified HA polymers with guest molecules (Adamantane - blue) and host molecules (β-CD - red). Figure adapted from Rodell et al[100].

The extent of supramolecular host and/or guest precursor modification can control their rheological properties; erosion and cargo profiles[102,103]. The polymer concentration, charge and competitive binding are factors that influence the properties of the supramolecular structure[104]. Low degree of modification of the polymer result in weak

supramolecular networks[104]. Interactions which are multivalent and interpolymer create a high avidity and network stability[105]. High levels of polymer modifications with the same host-guest molecules create robust supramolecular hydrogels because it results in a high avidity between polymers[100]. It has been shown that HA polymer chains with higher degrees of guest macromer modification showed a drastic decrease in crossover frequency (G'>G'' at lower frequency) when comparing to their less extensively modified counterparts[100].

C.1.1.2 Cavitands

A cavitand is a molecule that has the shape of a container, they can be naturally derived (*e.g.* cyclodextrins[106]) or synthetic (*e.g.* cucurbit[n]urils[107]; calix[n]arenes[108]; pillar[n]arenes[109]) (**Figure 6**).

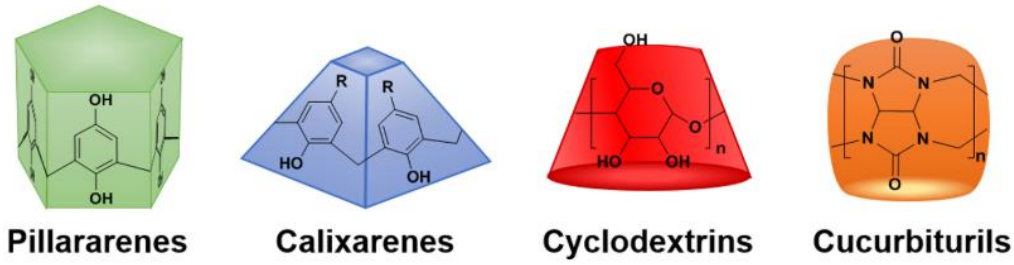

Figure 6 - Representation of cavitands host species and their monomer chemical structure. Figure adapted from Rodell et al[96].

Cyclodextrins (CD) have a cyclic structure made of D-glucose units arranged in a toroidal (resembles a doughnut) fashion through α-1,4 glycosidic bonds; the number of units varies between 6, 7 and 8 for α, β and ϒ CD, respectively (**Figure 7**)[106,110]. They contain a hydrophobic internal cavity that can accommodate hydrophobic guest molecules[106]. For this reason, cyclodextrins have been extensively exploited for the solubilization of hydrophobic drugs[111], and the design of supramolecular materials, including hydrogels[105].

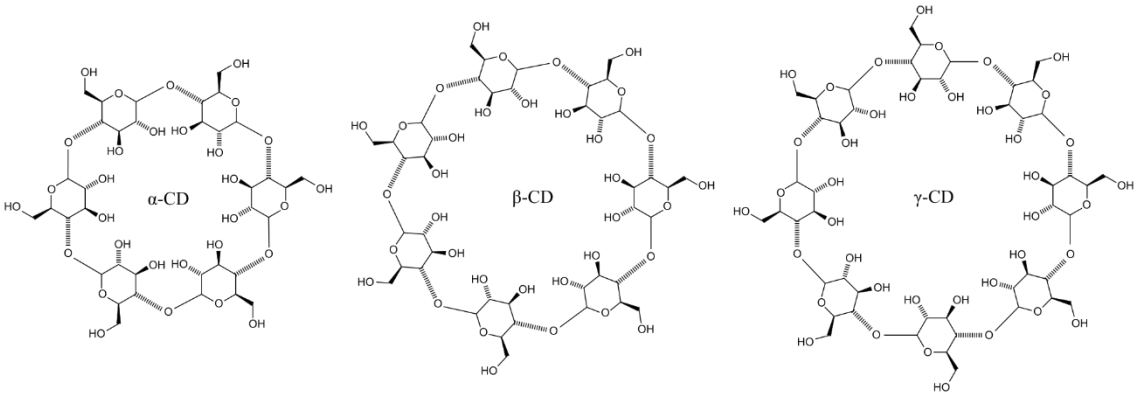

Figure 7 – Chemical structure of the three types of cyclodextrins: the α, β and ϒ CD, respectively. Figure from Nikitenko at al[110].

These molecules show high water solubility, low toxicity, have a long history of use, and their cavity sizes allow for a big range of guest hydrophobic molecules[96,106]. Furthermore, CD's enable scalability of synthesis because their synthesis, purification and modification processes have been optimized towards the industrial scale[96,106,112]. As a result, CD is a relatively inexpensive and abundant source of cavitands[96,106].

C.1.1.3 Printability

The printability[96,100,113] and degradation[96,100] behaviour of most host-guest assembled hydrogels can be described as follows (**Figure 8**):

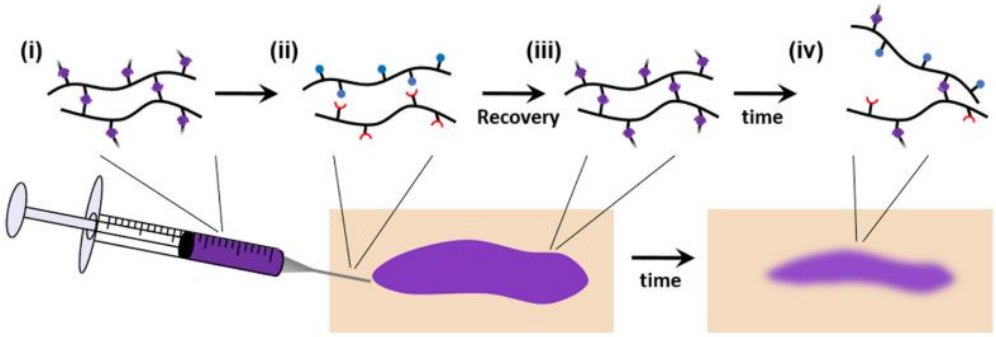

Figure 8 – Host-guest assembled hydrogel printing and degradation behaviour. Figure adapted from Rodell et al[96].

i) When there is no pressure being applied, the polymer chains interact through supramolecular interactions (purple), the material is cohesive.

ii) When pressure is applied, for example by a piston of a bioprinter, the supramolecular interactions break apart and the material becomes more fluid and is easily printed, thus showing a shear-thinning behaviour. This is the case for most supramolecular hydrogels since their physical bonds are broken upon the application of force.

iii) After printing, the pressure on the material stops, allowing for the host (red) and guest (blue) molecules to meet again. The material reassembles and regains its structure. Binding kinetics upon dispensing are important since a rapid bond formation equals to the material structure retention after dispensing.

iv) Host-guest hydrogels undergo natural disassembly due to their bond dynamic nature.

C.2 Chemical crosslinking

Chemical crosslinking includes methods for forming hydrogels by connecting the hydrogel precursors – low molecular weight monomers or polymeric building blocks –

through the formation of covalent bonds[3]. Chemical crosslinking can be tuned to achieve stable hydrogels with high mechanical strength[3].

Normally, the crosslinking reaction is initiated by mixing two gel precursor solutions (*e.g.* complementary reactive gel precursors)[3,114]. There is a wide range of possible chemical crosslinking mechanisms and some of them are depicted in **Figure 9**. Censi *et al.* covalently crosslinked thermosensitive methacrylate bearing polymers with thiolated hyaluronan using the Michael addition, which is catalyst-free reaction between the methacrylate and thiol groups that occurs at physiological conditions[115]. Additionally, gelatine and collagen biopolymers were crosslinked using 1-ethyl-3-(-3-dimethylaminopropyl) carbodiimide (EDC) and *N*-hydroxysuccinimide (NHS). EDC reacts with carboxylic groups (-COOH) creating an intermediate that will in turn react with primary amine groups ($-NH_2$)[116]. NHS is sometimes added to improve the efficiency of the reaction.

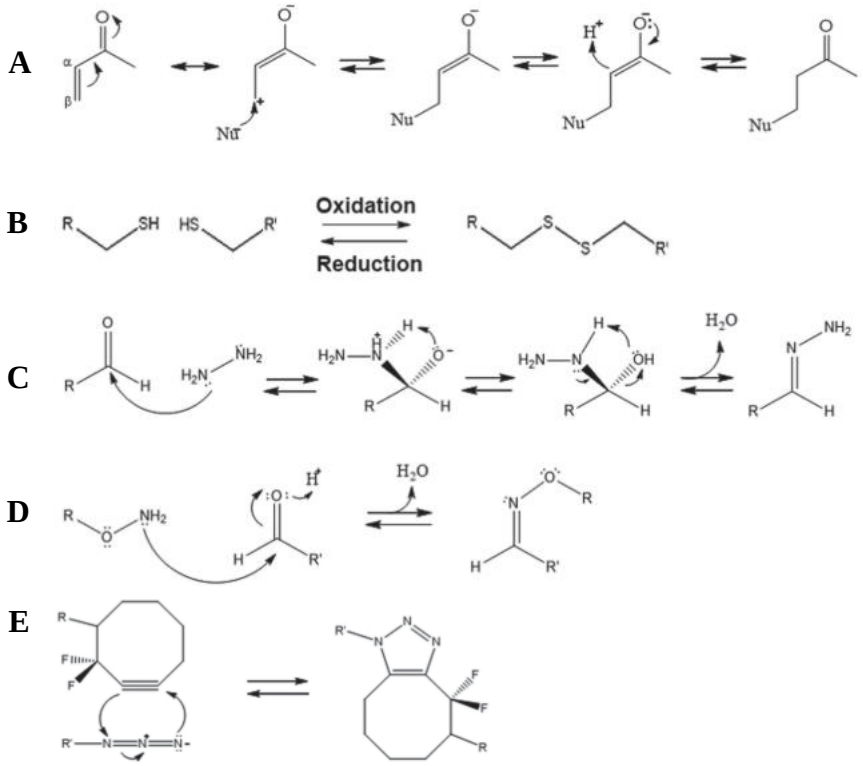

*Figure 9 – Chemical crosslinking mechanisms. **A**. Michael addition **B**. Disulphide formation **C**. Hydrazone condensation **D**. Oxime formation **E**. Diels-Alder cycloaddition. Figure adapted from Patenaude et al[114].*

The result is a constant increase in viscosity until the gel-point is reached and the 3D network develops. The downside of this strategy is the very strict control of crosslinking kinetics in order to not block the nozzle when going form the low viscosity printable precursor solution to the crosslinked hydrogel during the printing process[3]. However, shape fidelity needs to be guaranteed.

There are several different strategies to increase viscosity of the bioprinted gel each with their own setback:

1. Partial pre-crosslinking prior to deposition – however it is challenging to achieve the desired degree of crosslinking[117].
2. Initiation of the crosslinking process prior to printing – it also ensures a reduction of the gelation time, however, the continuous change in rheological properties during printing may very well affect the final printing fidelity[3,118].

Due to the above-mentioned problems, chemical crosslinking is mainly used for the stabilization of the printed construct. Typically, by fixating a weakly physical crosslinked printed construct[119]. This can be done in several ways such as post-processing reaction of complementary chemical groups[120].

Another alternative is the use of photo-crosslinking because it gives temporal control over the reaction. This strategy allows for the material to be crosslinked either during or after printing[119,121]. The post-processing of the photo-polymerization step can cause a very fast crosslinking, thus ensuring shape maintenance immediately after printing[119].

Furthermore, the crosslinking process should not be harmful to cells and thus be developed under mild/physiological conditions with chemistry that is compatible with bioactive proteins and living cells. This means that it should avoid the production of toxic by-products and the use of non-biocompatible monomers and hydrogel precursors.

D. Bioinks

A bioink is a soft biomaterial loaded with living cells, essentially it is the "raw material" of bioprinting processes[77]. It allows for the manipulation of the biological and biochemical environment and incorporation of living cells to create complex biological constructs[77].

As mentioned before, cells require a support material in order to survive and proliferate[4]. Hence, the process of bioprinting – defined as the placement of cell embedded biomaterials into spatially defined structures using automated 3D bioprinter technologies - requires a delivery medium for cells so that they can be deposited in the desired shape[77].

A good bioink is expected to be deposited easily and form a bioprinted construct that maintains its shape and structural strength for a defined period *in vitro* and easily engraft in the host and degrade over time *in vivo*[77]. Additionally, a bioink should be able to

maintain cell viability during short and long-term culturing; cell spreading and proliferation; cell-cell and cell-ECM interactions and exhibit good post-printing functionality[77].

As such, to fulfil its function a bioink should be[4]:

1. Viscoelastic: To allow for the appropriate fluidity for cell protection within the nozzle as well as an increase in the printing definition and post-printing stability[122,123].
2. Have good bioprintability – Have appropriate fluidity to allow dispensing while preserving the viability of the embedded cells[122,123].
3. Have good mechanical properties – Have the shape, mechanical stability and integrity simulating that of a certain tissue while offering structural support and physical environment for cells to attach, grow, migrate and respond to signals[4].
4. Biocompatible: Non-toxic and non-immunogenic[77]. The biomaterial needs to be compatible with the embedded cells as well as the endogenous cells in the host tissue[6].
5. Bioactive: Interact with embedded cells to facilitate and regulate cellular activities through the presence of biomolecules such as growth factors[4] and have polymer sequences to which cell can adhere[77].
6. Biodegradable: Allow new tissue formation and remodeling to facilitate integration in the host tissue[4].

There are two major types of materials used as bioinks for 3D bioprinting of tissues and organs[124]. The scaffold-based and the scaffold-free bioink materials.

In scaffold-based bioinks cells are loaded onto a soft biomaterial such as decellularized matrix components[7,125], microcarriers[126] or hydrogels[7] prior to being bioprinted into a 3D construct.

On the other hand, scaffold-free bioinks, do not use any exogenous biomaterial to print cells, instead cells are deposited in specific patterns (*e.g.* using a mould such as a capillary micropipette) and eventually fuse together and form a larger tissue by secreting ECM components that will hold them together[127,128]. Thus, mimicking the embryonic development[77]. The formed tissue can either be 3D-bioprinted or grown into the final shape of the construct.

The advantages of the scaffold-free bioinks is that since it is made solely by cells it bypasses several problems that arise when using scaffolds, such as: immunogenicity, inflammatory response, mechanical and biochemical mismatch with the surrounding tissue which can affect negatively, in the long-term, the behaviour of the engineered scaffolds and its primary biological function[127].

E. Additive manufacturing

Additive manufacturing (AM) technology has been used to create bio-engineered 3D structures that mirror the complexity of native tissues[129]. It uses medical imaging techniques or other 3D model data sets to generate personalized specific computer-aided designs to create scaffolds with detailed geometries using a layer-by-layer assembly methodology[130–132]. Hence, this technology allows for the fabrication of anatomically shaped implants and customized constructs. Moreover, because it is a computerized technique it offers a high level of control over the structure of the fabricated construct; reproducibility; and allows for scale-up and standardization of the process[129].

AM technologies can spatially direct the material to form the 3D model, by fixing its shape, using one or several processes simultaneously which are: thermal, chemical, mechanical and/or optical (**Table 3**)[129].

Table 3 - AM techniques used in tissues engineering with their characteristics. For processing modes, t – thermal; m – mechanical; c – chemical and the modes in brackets are optional. Image adapted from Melchels et al[129].

Technique	Processing modes	Accuracy (μm)	Materials	Cells
Inkjet printing (thermal or piezo-electric)	t/m, (c)	20–100	Liquids, hydrogels	Yes
3D printing	m, (c)	50	Polymers, ceramics	No
Stereolithography (incl. two-photon polymerization)	o, c	0.5–50	Hydrogels, polymers, ceramic-composites	Yes
Laser direct writing	o	20	Cells in media	Yes
Direct writing	m, c	1	Polyelectrolytes	Not yet
Melt extrusion (including FDM)	t, m	200	Thermoplastics, composites	No
Extrusion bioprinting/ Robotic dispensing	m, (t), (c)	100	Hydrogels, polymers, ceramic-composites	Yes
Selective laser sintering	o, t	50	Polymers, ceramics	No
Biolaserprinting	o, t	10	Liquids	Yes
Robotic assembly	m	5	Rigid solids	Not yet

Additionally, cells and/or growth factors can be incorporated into these computer-controlled fabrication processes to create 3D constructs with a specific spatial cellular arrangement[133–136] although only some of the mentioned techniques are cell friendly.

E.1 Printability

The printability of hydrogel precursors is determined by their physico-chemical parameters (*e.g.* rheological properties) and the target bioprinting modality because each bioprinting modality has different bioink requirements due to differences in the processing parameters (*e.g.* nozzle gauge)[3].

Firstly, the embedded cells need to survive the bioprinting process. Secondly, the bioprinted construct needs to have mechanical stability and shape fidelity. This can be achieved by, for example, post-printing processing like gelation resultant from crosslinking.

There are essentially three bioprinting modalities for hydrogel bioprinting: the inkjet bioprinting, the orifice free bioprinting and the extrusion bioprinting (**Figure 11**)[137].

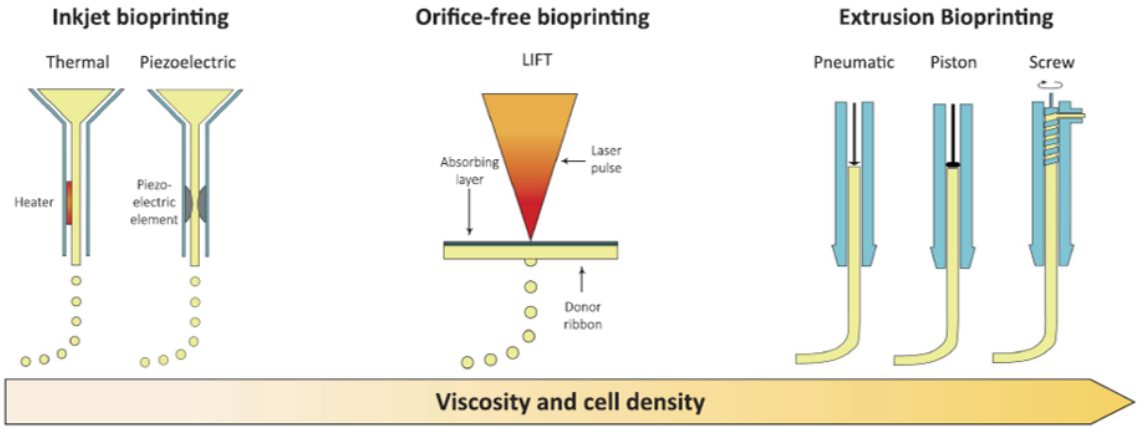

Figure 10 - Different modalities for hydrogel bioprinting namely: Inkjet; Orifice-free and Extrusion bioprinting. Characterization of their relative bioink viscosity and cell density. Figure adapted from Hölzl et al[137].

The Inkjet bioprinting consist of the deposition of small volumes (picolitres) of bioink (*e.g.* culture media and/or hydrogel) expelled into a substrate by either heat (thermal) or a direct mechanical impulse - shock wave (piezoeletrectric)[136].

In the orifice-free bioprinting modality, comprised by the laser-induced forward transfer (LIFT) bioprinting technique a donor substrate (made of an absorbing layer and a layer of bioink) is irradiated by a laser. The focused laser pulses evaporate the absorbing (e.g. gold or titanium) which creates a high vapor pressure that in turn propels the bionk into the collector[138].

Lastly, for extrusion bioprinting (EB)[137] (also called robotic dispensing[3]), hydrogel embedded cells are inserted in disposable plastic syringes and dispensed, as large hydrogel strands, on a building platform by a pneumatic, piston or screw driven force[3].

E.1.1 Extrusion bioprinting

The extrusion bioprinting (EB) technique uses mechanical processing and allows for the formation of a 3D model with multiple compositions. It is used with polymers, ceramic-composites and hydrogels[129].

In EB, high viscosity bioinks can be used, their viscosity ranges from 30 mPa/s to $6x10^7$ mPa/s[139]. The bioink should also show shear-thinning behaviour to allow easy flow through the nozzle. High viscosity hydrogels are often used in order to maintain the shape of the construct after printing hence giving time for post-processing cross-linking the construct[3]. Cell density can affect bioink viscosity, a higher cell density increases a hydrogels viscosity and allows for the bio-impression of hydrogels with very high cell densities including spheroids[139].

Piston-driven systems give more control to the flow of the bioink as opposed to pneumatic-driven systems due to the delay associated with the gas volume compression[137]. Screw-driven systems provide the most control over spatial bioprinting and extrude the highest viscosity bioinks though, this system can harm cells by disrupting the cell membranes due to the large pressure drops that it generates[3].

EB has an accuracy in the order of 100 μm which is relatively low when comparing with other techniques (**Table 10)**[129]. However, this type of approach is significantly faster[3]. Other disadvantages of EB are the possibility of nozzle clogging and decreased cell viability due to shear stress[140].

Overall, EB allows for the creation of 3D constructs with a clinically relevant size within a realistic time frame[3].

F. Rheology

Rheology studies show how mater flows when an external force is applied to it[3]. Thus, it is highly relevant to 3D bioprinting. The most used rheological measurements to characterize and select suitable candidates for 3D-printing are[141,142]:

1. Steady-shear flow curves (*i.e.* apparent viscosity vs shear rate);
2. Oscillatory data (*i.e.* viscous and elastic modulus vs angular frequency);
3. Creep and recovery curves (*i.e.* viscous and elastic modulus vs time);
4. Temperature sweeps (*i.e.* viscous and elastic modulus vs temperature).

These tests are commonly run due to the relationship between a material mechanical characteristic and its 3D printability[142]. Proper rheological characterization is very important in extrusion bioprinting, because it is crucial for selecting the best processing conditions and understand the potential framework of application of a material[142]. Additionally, inks used in this type of bioprinting should show additional features, that can be observed through rheological measurements, such as: shear-thinning behaviour[143].

F.1 Viscoelasticity

Most of the biological tissues and its components (*e.g.* cells; extracellular matrix; structural proteins; among others) possess viscoelastic mechanical properties which are important for their functionality[144].

A viscoelastic material response has characteristics of both elastic and viscous materials (**Figure 11**).

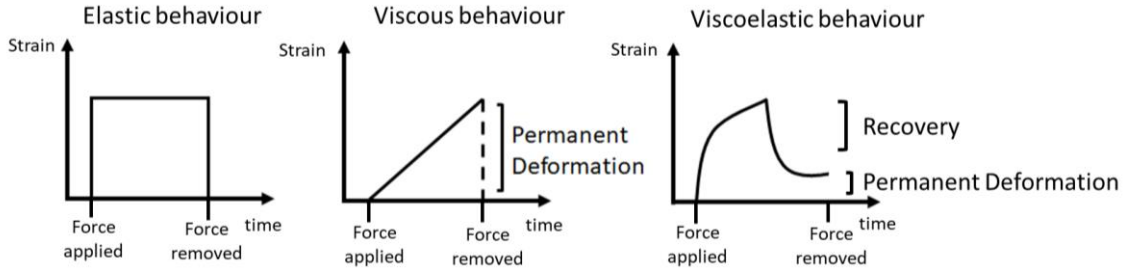

Figure 11 – Behaviour of elastic, viscous and viscoelastic materials to an applied stress. The strain axis refers to the materials response (deformation) to an applied stress. Reproduced from[145].

F.1.1 Elasticity

Upon application of an external force an elastic material will generate a recovering force (an inner force) which creates a resistance to the applied force. When the external force is eliminated, the material regains its initial form and the recovering force ceases to exist[144]. Thus, elasticity is a material property to resist deformation by an external force.

F.1.2 Viscosity

Viscosity, a material property of a fluid, is the resistance of a fluid to flow upon application of stress[144]. However, unlike elasticity, when the deforming force stops, thus stopping the flow, the material maintains its deformation when the force is released[144].

The shear stress is related to the amount of force applied per area to cause a deformation in the fluid (or flow). Lastly, the shear rate is quantified by the rate of displacement of the

fluid or the rate of flow. Altogether, the viscosity relates with shear stress and shear rate by the following **equation (a)**[146]:

$$(a) \quad viscosity = \frac{Shear\ stress}{Shear\ rate}$$

Shear stress, in 3D bioprinting, is related to higher speeds of flow rate and the geometry of the dispensing setup (nozzles, orifices and channel dimensions)[3].

Viscosity of the polymer is determined by polymer concentration and molecular weight. High polymer concentrations are limiting in terms of cell compatibility because they create a restrictive environment for cell proliferation, migration and tissue formation[3].

Thus, most researchers opt for a high molecular weight polymer which requires less polymer concentration to obtain the same level of viscosity of the final product[3].

In 3D bioprinting, high viscosity prevents the formation of a surface tension-driven droplet formation - which facilitates filament-based deposition - and the collapse of the printed construct[3].

The viscosity of the hydrogel forming solution dictates how quickly it needs to solidify since it influences the shape fidelity after deposition[3]: low viscosity solutions tend to form droplets at the needle tip which results in the deposition of strands that spread out on the surface, while high viscosity solutions form filaments rather than droplets[147].

It is then an intuitive conclusion that printing fidelity increases with increased viscosity; however higher viscosity requires the application of a higher shear stress (See **equation (a**) which might harm the embedded cells[148].

Long-term studies on the influence of intermediate shear stress on cell attachment and behaviour have shown a clear detrimental effect[149,150]. Endothelial cells seeded onto Dacron membranes subjected to a range of shear stress for up to 24h, shown a decrease detachment and apoptosis after 6h[150]. Additionally, shear stress influences chondrocyte metabolism and resulting in an increase in apoptosis[149].

Short-term studies, show that the exposure to high shear stresses that may arise from 3D bioprinting does not seem to have a high impact in cell viability[3,151,152]. Namely, Khalil *et al.* measured cell viability of endothelial cells in a solution of sodium alginate extruded through a pneumatic nozzle and determined that 83% of the cells encapsulated in the scaffold were viable[152]. Moreover, Saunders *et al.* studied the effects of shear stress on

fibroblasts using inkjet bioprinting technology and the results showed a 98% and 94% survival rate with a 40 V and 80 V pulse, respectivelly[151].

In extrusion bioprinting, a negative impact in cell viability can be correlated to shear stress which increases with higher printing speeds and thinner nozzles[153]. A reduction of shear stress would mean lower resolution – larger orifices/nozzles - and the reduction of the flow rate[3]. Thus, a balance between these parameters needs to be achieved.

F.2 Shear thinning

Shear thinning describes the decrease in viscosity as shear rate increases, due to the shear induced reorganization of the polymer chains to a more stretched conformation, which results in lower entanglement, hence viscosity[100,113].

Shear-thinning is displayed by most polymers, especially high molecular weight polymers (*e.g.* alginate[154]). Additionally, the higher the polymer concentration the more accentuated the material shear thinning is, since there is a greater relative reduction of viscosity induced by shear[3,119].

Shear thinning behaviour is highly relevant during bioprinting. Indeed, in the nozzle, where there is a high deformation of the material – high shear rates - the viscosity decreases and so does the shear stress, while upon deposition the viscosity increases sharply due to the abrupt absence of shear rate. Thus, shear thinning increases printing fidelity[3].

F.3 Yield stress

Yield stress determines the amount of force (in 3D bioprinting – shear forces) that needs to be applied to the material to initiate a flow[3].

Normally, when two polymer chains interact, a physical network is formed, which is fragile and can be readily broken by shear forces (during printing) above the yield stress. When the shear force is removed, the material slowly regains its structure[100].

While highly viscous materials only delay the collapse of the deposited 3D construct, the presence of a yield stress can potentially prevent flow and collapse of the structure as well as improve printing fidelity and prevent cells from settling in the hydrogel precursor reservoir[3].

Project's background

Currently, in the field of tissue engineering there is a growing need for alternative methods to create tissues and organs with the required structural, mechanical, and biological complexity[152]. This need arises from the existing shortage of tissues and organs for transplantation, as well as tissue models for drug discovery and testing[155].

3D bioprinting allows for the construction of scaffolds with high complexity (*i.e.* their design can be based on medical images[129]) which can be customed and patient specific. Furthermore, 3D bioprinting techniques can be optimized in order to be low-cost and highly efficient[156]. In extrusion 3D bioprinting the bioink should come out of the micronozzle smoothly with minimal pressure; however, after extrusion it should undergo rapid gelation with minimum deformation and allow for cell viability[157].

Despite the attention that the field has received, the search for a suitable biomaterial remains a challenge because bioinks need to be simultaneously fine-tuned to be biocompatible, printable (good rheological properties) and possess biomimetic properties for the targeted native tissue, such as mechanical and structural stability[158].

To this end, biomaterials (*i.e.* hydrogels) made of a blend of silk and gelatine polymers have been investigated due to their complementary characteristics. While silk provides good mechanical properties and tailored degradability, gelatine is used as a bulking agent (*i.e.* to increase viscosity) and to increase the biocompatibility of the ink, since it possesses cell-adhesive motifs (absent from silk chains), due to its natural origin, that support tissue growth[80,157,159].

Previous studies have described blends of silk - gelatine formulations , either with[157,159] or without[80] crosslinking agents. Some of the crosslinking agents used were: mushroom tyrosinase[157], sonication[157], ethanol and methanol[159]. However, the use of crosslinking agents may increase the scaffolds toxicity and/or induce structural alterations. Thus, the choice of a suitable crosslinking mechanism that is mild and cell friendly is of utmost importance.

Furthermore, a biomaterial with shear-thinning behaviour is advantageous for 3D extrusion bioprinting because it allows for an ease in extrusion while, simultaneously, enabling the material to regain its shape once it is extruded (*i.e.* low shear forces). Rodell *et al.*, has used host-guest supramolecular chemistry to create injectable hydrogels that possessed the desired shear-thinning and self-recovery behaviour[100].

Moreover, CD has been shown to be a good cavitand (host molecule) because it is able to interact with several guest molecules such as the aromatic ring on tyrosine residues (Tyr)[160] (**Figure 12**) both present in the gelatine[161] and silk[33] polymeric chains.

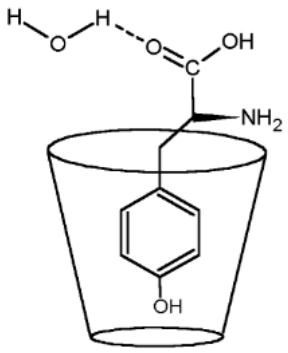

Figure 12 – Tyrosine residue inclusion on the β-CD molecule. Figure adapted from Shanmugam et al[160].

However these type of physical crosslinking mechanisms result in a less mechanically robust hydrogel[100]. To circumvent this setback, post-printing chemical crosslinking is used as strategy to stabilize the construct. This strategy ensures shape maintenance immediately after printing and allows for the preservation of the mechanical properties of the constructs for longer periods of time[119]. The latter is important to provide the required time for matrix remodelling *in vivo* with synchronized construct degradation and native extracellular matrix regeneration[68,69].

Due to its biocompatibility, a visible light based crosslinking mechanism, which uses riboflavin as a photo-initiator[162], can potentially be a good strategy for structural post-printing photo-stabilization of a bioink.

Objectives

The current project aims to develop a novel self-healing biomaterial ink for 3D bioprinting based on silk and gelatine. To this end the main objectives of the project are:

1. The synthesis of CD functionalized gelatine;
2. Characterization of Silk-Gelatine blends using different ratios of the biopolymers regarding their:
    a. Rheological properties
    b. Printability - by 3D printing using an extrusion based bioprinter, the Silk - Gelatine blend

Materials and methods

Silk fibroin extraction

Silk cocoons were obtained from Evrosilk (Žďár nad Sázavou, Czech Republic). Silk fibroin extraction procedure was based on Rockwood *et al*[27] with some modifications. Briefly, silk cocoons were boiled for 5, 10 and 30 min in a 0.02M solution of sodium carbonate (Na_2SO_3, Merck, EMSURE® ISO, Germany). Silk fibroin was dried overnight before being dissolved at 15% w/v in a solution of 9.3M LiBr, Thermo Fisher Scientific, Acros Organics, Germany) and left slowly stirring at 70°C for 2.5 hours. Silk fibroin solution was dialysed, in 3.5 kDa cut-off dialysis tube (Pur-A-Lyzer™ Mega 3500 dialysis kit, Sigma-Aldrich, Israel), against ultrapure water overnight. Dialysis water was changed every half an hour for a total of 4 times/day. The dialysed silk solution was centrifuged twice at 4°C for 20 min at 9000 rpm to remove any debris before being stored at 4°C.

Silk fibroin concentration

The previously dialysed silk solution was concentrated by dialysis 20% w/v PEG (10000, Sigma-Aldrich, Fluka® Analytical, Germany) overnight at 4°C. The concentrated silk fibroin solution was stored at 4°C.

Synthesis of succinyl-β-cyclodextrin functionalized gelatine

Half a gram of gelatine (Porcine skin, Type A, Strength 300, G2500-500G, Sigma-Aldrich, USA) were dissolved in 10 mL of Borax (sodium tetraborate tetrahydrate) buffer (pH 8.5, Sigma-Aldrich) and heated at 40 °C while stirring, followed by addition of 1 ml of Dimethylformamide (DMF, Merck, EMPLURA®, Saudi Arabia) and stirring at room temperature. Separately, 0.25 mmol of succinyl-β-cyclodextrin (S-β-CD, Cyclodextrin-Shop, The Netherlands) were dissolved in 2 mL of anhydrous DMF. Then, 0.5 mmol of EDC (Thermo-Fisher Scientific, Alfa Aesar, Germany) were added to the S-β-CD solution and left stirring for 30 minutes at 0°C. After 30 min, the activated S-β-CD solution was added to the stirred gelatine solution dropwise. The reaction proceeded for 2 h at room temperature. The product was precipitated with acetone (VWR Chemicals, France), dissolved in phosphate-buffered saline (PBS) buffer (pH=7.4) (Sigma-Aldrich, USA) at 40°C and re-precipitated.

S-β-CD functionalized gelatine was washed with cold water twice before being dissolved in ultrapure water at 40°C and lyophilized (Alpha 1-2 LD plus, Salm en Kipp, The Netherlands).

Adsorption assay

The adsorption assay was carried out using basic fuchsin (BF, Basic Violet 14, Klinipath, The Netherlands). To calculate the amount of fuchsin in solution, a fuchsin standard curve was prepared (0.00025 – 0.0312 mg/ml). The absorbance values were measured at ʎ=543 nm using a microwell plate reader (VersaMax™ tunable microplate reader, Molecular devices).

For each sample (1 mg/ml), 100 µl were pipetted into a 1.8 µl fuchsin solution (0.0312 mg/ml). The mixture was vortexed and incubated for 2h at room temperature. Afterwards, the mixture was spun down for 5 min and 50 µl of the supernatant were pipetted into a 96-well plate along with 150 µl of ultrapure water.

The equilibrium adsorption capacity ($A_{c\ eq.}$) of the samples was determined using the following **equation (b)**, adapted from Zhang *et al.*[163]:

$$(b) \qquad A_{c\ eq}\,(\mathrm{mg/g}) = \frac{C_0\,(\mathrm{mg/ml}) - C_e(\mathrm{mg/ml})}{m\ (g)} \times V\ (ml)$$

Where C_0 (mg/ml) is the initial concentration of BF; C_e (mg/ml) is the equilibrium concentration of BF; m (g) is the mass of adsorbent present in the sample; and V (ml) is the volume of the BF dye solution[163].

2,4,6-Trinitrobenzenesulfonic acid assay

The 2,4,6-Trinitrobenzenesulfonic acid (TNBS) assay was performed using the Habeeb method[164]. Briefly, 25 µl of gelatine solution (5 mg/ml and 2.5 mg/ml of modified (GelM) and unmodified (Gel) gelatine); 25 µl of sodium hydrogen carbonate solution (N_2HCO, 4% w/v, pH= 8.5, Sigma-Aldrich, USA) and 25 µl of TNBS (0.1% v/v, Sigma-Aldrich, USA) were pipetted into a 96-well plate before being incubated for 2.5h at 37°C in the dark. After incubation, 25 µl of sodium dodecyl sulphate (SDS, 10 % w/v, Sigma-Aldrich, Japan) were added to solubilize protein and prevent its precipitation upon de addition of 12.5 µl of hydrochloric acid (HCl) solution (1 mol/l, Sigma-Aldrich, EMSURE®, Germany). Absorbance was measured at ʎ=346 nm on a microwell plate reader (VersaMax™ tunable microplate reader, Molecular devices). The calculation of the amino group content was done using a glycine (MP Biomedicals, Inc.) standard curve (0.02-2.5 mmol/l).

The degree of modification measured using the TNBS assay (DM_{TNBS}) was calculated using **equation (c)** which was adapted from Claaßen *et al.*[165].

$$(c) \quad DM_{TNBS} = NH_2\ content\ Gel\ \left[\frac{mmol}{g}\right] - NH_2\ content\ GelM\ \left[\frac{mmol}{g}\right]$$

Gel casting

Solutions with different ratios of silk and gelatine or S-β-CD functionalized gelatine were prepared and mixed with a final concentration of 2mM Riboflavin 5'-monophosphate sodium salt hydrate (RBFM, Sigma-Aldrich, France), and 20 mM sodium persulfate (SPS, Honeywell Research Chemicals, Germany).

After gentle mixing, 100 µl of the prepared solutions were placed on a mould and exposed for 15 min to visible light (LED slim food light 20W 6400K AC200-240V/50Hz, Aigostar).

Swelling ratio and sol-fraction

Gels were sequentially freeze dried, incubated in 1 ml of ultrapure water at 37°C for 24h and freeze dried again.

The swelling ratio and the percentage of sol-fraction of the casted gels was determined using the following **equations (d)** and **(e)** respectively, adapted from Guo *et al.*[91]:

$$(d) \quad swelling\ ratio = \frac{Ws - Wd}{Wd}$$

$$(e) \quad \text{sol-fraction } (\%) = \frac{Wi - Wd}{Wi} \times 100$$

Where W_i is the weight of the dried gel after cross-linking; W_s the weight of the gel after swelling in water; and W_d the weight of the dried gel after swelling.

Rheological characterization

The rheological measurements were performed using a discovery hybrid rheometer HR-2 (TA-instruments) fitted with a 20 mm diameter aluminium plate with solvent trap (Part number: 513200.905, TA instruments, UK). The viscosity of the different polymer solutions was measured with a shear rate range from 1 to 900 s^{-1} at 25°C. Rheological properties of the crosslinked hydrogels were examined at 25°C by oscillatory frequency sweeps (0.1-15 Hz; 1% strain), oscillatory strain sweeps (0.5-600% strain; angular frequency of 10 rad/s). Further, shear recovery experiments were performed by varying the

strain from 500% to 1% strain, each at 1 Hz. Unless otherwise stated, all rheological tests were performed on three different samples.

Calculation of the structural parameters

The rheological measurements can be used to evaluate the average mesh size of the hydrogels. The average mesh size (nm) is defined by the distance (Å) between the cross-linking points and can be calculated, based on the rubber elastic theory (RET), using the following **equation (f)**[166]:

$$(f) \quad mesh\ size = \left(\frac{G' N_A}{RT}\right)^{-1/3}$$

where the G' is the storage modulus, N_A is the Avogadro constant (6.022×10^{23}), R is the gas constant (8.314 J/K mol) and T is the temperature in Kelvin (298.15K).

The crosslinking density (n_e) of the hydrogels describes the number of elastically active junctions in the network per unit volume (mol/m^3) and it can also be calculated based on the RET with the following **equation (g)**[166]**:**

$$(g) \qquad n_e = \frac{G_e}{RT}$$

where G_e is the peak value of the G' storage modulus in the linear viscosity region (LVR) measured by the frequency sweep test.

It is also possible to calculate the average molecular weight of the polymer chain between neighbouring crosslinks (M_c, kg/mol) through the following **equation (h)**:

$$(h) \qquad M_c = \frac{c\rho RT}{G_e}$$

where c is the polymer concentration (5 – 7.5 % w/v) and ρ is the density of water at 298.15 K (998.2071 kg/m^3)[167].

Polymer extrusion bioprinting

A pneumatic, dual extruder 3D bioprinter (INKREDIBLE, CellInk AB, Sweden) was used to test the printability of different silk: S-β-CD-gelatine blends. The 3D printing software Slic3r was configured with an INKREDIBLE bioprinter. Straight high precision blunt nozzle needles (Precision stainless steel tips, Nordson EFD) were used in all experiments.

Statistical analysis

The data was analysed using JMP software. An unpaired student t test was used to determine whether a significant difference existed ($p < 0.05$) between the different groups.

Results and Discussion

Synthesis of succinyl-β-cyclodextrin functionalized gelatine

The functionalization of gelatine with β-Cyclodextrin[168] (β-CD) was achieved using S-β-CD[169] (**Figure 13 - A**). The succinyl molecules provide carboxyl groups (-COOH) which can be activated by EDC[170] in order to be connected to primary amine groups (-NH_2) of the lysine residues of gelatine (**Figure 14**).

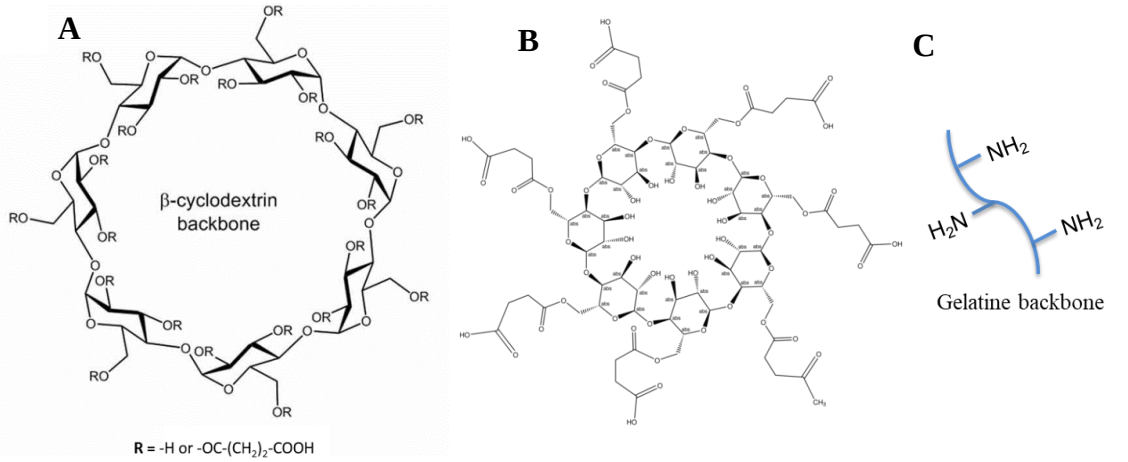

Figure 13 – β-cyclodextrin (β-CD) molecules: ***A.*** *The backbone of β-CD. When R=H then the molecule is β-CD; if R=-OC-$(CH_2)_2$-COOH the molecule is succinyl- β-CD (S-β-CD).* ***B.*** *S-β-CD molecule.* ***C.*** *Gelatine backbone with primary amines (NH_2) attached to its polymeric chain. Figure 14.A and B were adapted from Crumling at al[168] and [169], respectively.*

The activation of S-β-CD with EDC (first step in the reaction) was performed using an organic solvent to decrease the degree of hydrolysis of the EDC activated S-β-CD (**Figure 14**) and to increase the solubility of the S-β-CD mixture.

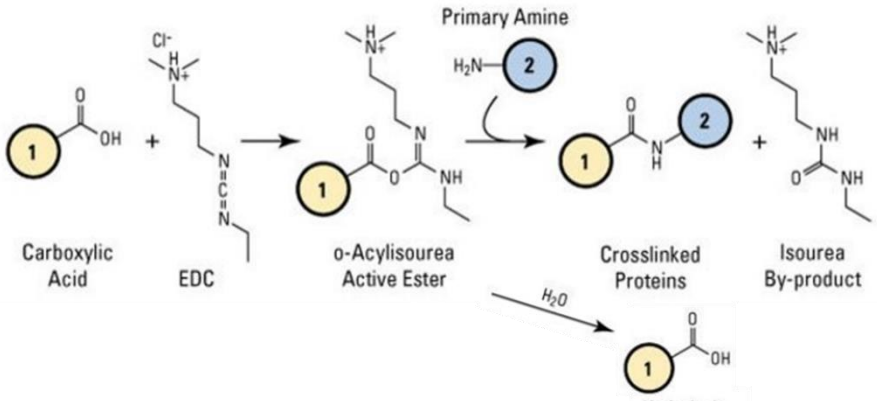

Figure 14 - Reaction scheme for carboxyl-to amine crosslinking with the carbodiimide EDC. Molecules 1 and 2 are S-β-CD and gelatine, respectively. Figure adapted from [170].

To assess if S-β-CD was successful conjugated to gelatine, two assays were performed, namely the fuchsin assay and the TNBS assay.

Fuchsin assay

Fuchsin has a structure composed by three aromatic rings combined with a carbon (**Figure 15**) which can be difficult to be adsorbed[163].

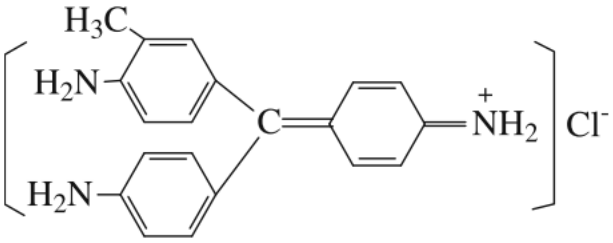

Figure 15 – Chemical structure of fuchsin. Image taken form Zhang et al[163].

However, β-CD is able to adsorb fuchsin[163]. When fuchsin is mixed with a solution containing β-CD it is expected that most of the fuchsin will be collected as pellet following centrifugation. The amount of fuchsin present in the supernatant can be measured spectrophotometrically allowing for the calculation of the adsorption capacity of a sample.

The values of adsorption capacity of a S-β-CD, a Gel and GelM solutions were measured and the data are presented in **Figure 16**.

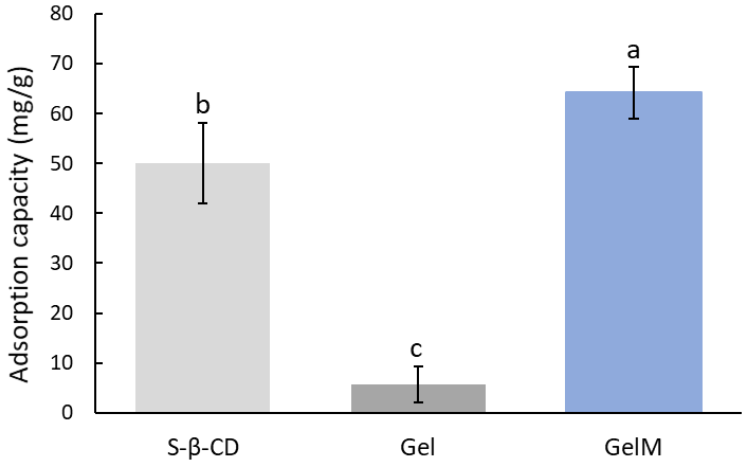

Figure 16 – Bar-plot of the adsorption capacity of samples of S-β-CD (average ± sd), non-modified and modified gelatine per mass of adsorbent. The results presented are an average of three technical replicates (n=3). Bars with different letters differ p<0.05.

The adsorption capacity of S-β-CD, Gel and GelM solutions was of 50.05 ± 8.09, 5.76 ± 3.60 and 64.16 ± 4.47 mg/ml respectively (**Figure 16**). The S-β-CD solution has a higher adsorption capacity when comparing to the Gel solution. This can be explained by the presence of β-CD, in the S-β-CD solution, that entraps the fuchsin molecules while the Gel solution is devoid of β-CD, thus unable to held captive the soluble fuchsin molecules.

However, the adsorption capacity in the Gel solution is not null, most likely because the gelatine polymers can intertwine and create a loose mesh that is able to entrap a small quantity of fuchsin molecules.

The GelM solution shows the highest adsorption capacity, that might be explained by the combined effect of the loose gelatine mesh and the adsorption of fuchsin by the β-CD molecules. Therefore, this assay shows that gelatine was successfully modified with CD.

TNBS assay

To further determine if the S-β-CD was successfully attached to gelatine's polymeric chain and the degree of this modification, a TNBS assay was performed. TNBS can form a covalent bond with the free NH_2 groups of gelatine, indicated by a change of colour of the solution, that can be measured spectrophotometrically (**Figure 17**)[171].

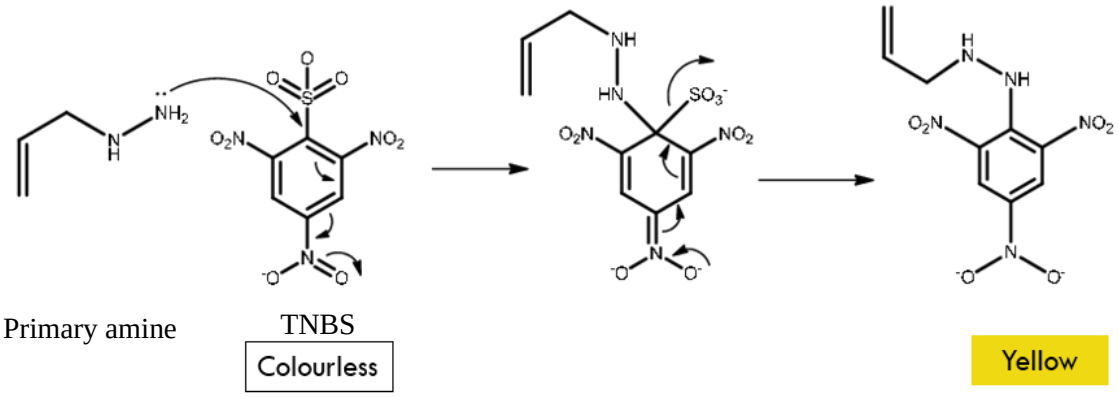

Figure 17 – TNBS reaction with a primary amine accompanied by a change in coloration of the compound. Figure adapted from Perng et al[171].

Since the -COOH groups of succinyl attach to the -NH_2 groups of gelatine, the difference between the amount of free -NH_2 groups in Gel and GelM samples can be used to determine the degree of modification (**Figure 18**). It is important to mention that two types of phenomena can happen when S-β-CD attaches to the gelatine chain, as shown in **Figure 18**:

1. one molecule of S-β-CD may attach to one gelatine chain through one or several succinyl groups;

2. one molecule of S-β-CD may attach itself to 2 or more gelatine chains.

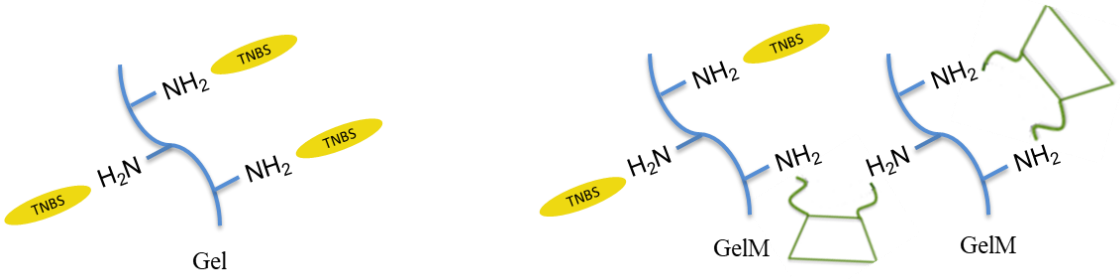

Figure 18 – Interaction of TNBS with the free primary amine of non-modified (Gel) and modified (GelM) gelatine.

The amount of free primary amine groups per gram of sample, in this case Gel and GelM is shown in **Figure 19**.

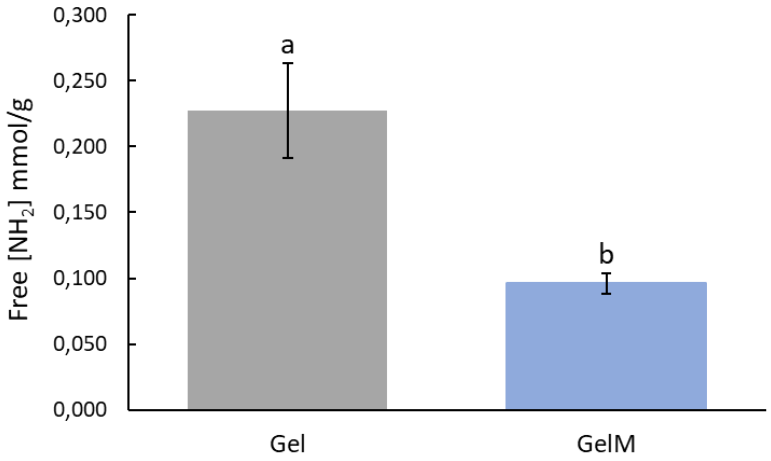

Figure 19 –Bar-plot of the amount of free primary amines (NH_2, average ± sd) in non-modified (Gel) and S-β-CD modified (GelM) gelatine, respectively, per mass of gelatine. The results presented are the average of three technical replicates (n=3). Bars with different letters differ p<0.05.

The amount of free primary amine groups was calculated, Gel and GelM had 0.227 ± 0.036 and 0.096 ± 0.008 mmol/g of free NH_2 groups per mass of gelatine, respectively (**Figure 19)**. As expected, the amount of free NH_2 groups is higher for Gel in comparison to GelM. This result agrees with the fuchsin assay data, both showing that gelatine was successfully modified.

The DM_{TNBS} = 0.131 mmol/g of S-β-CD bound NH_2 groups per mass of gelatine, and the degree of modification in percentage was of ~42%.

Silk - Gelatine blends

Silk, used in subsequent experiements, was boiled for different time points (5, 10 and 30 min). The longer silk is boiled the lower its final molecular weight (MW)[172]. Thus, the

expected gradient size for the silk polymer chains in the present experiment are: 5 min > 10 min > 30 min. The silk polymer chain size obtained by Singh *et al.* in silk boiled for 10 min was ~171 – 460 kDa and 30 min was ~31 – 268 kDa[172].

Additionally, the different silk solutions were mixed with both GelM and Gel solutions in order to determine the effect of the addition of CD to gelatine.

Rheological characterization: Silk – Gelatine solution

Viscosity

For EB, bioinks should be highly viscous, to maintain the constructs shape after printing, and show shear-thinning behaviour for an ease of extrusion[3,139]. Since higher MW polymers have higher viscosity, the silk used in this experiment was the one boiled for 5 min.

GelM was added to the silk regenerated solution because it is expected that the CD on the gelatine's polymeric chain creates host-guest supramolecular interactions with the tyrosine residues on silk chains. These physical, reversible interactions should contribute to an increase in viscosity and shear-thinning behaviour of the overall blend.

Viscosity measurements were conducted on Silk, GelM and Silk-GelM solutions to evaluate the effect on viscosity and shear-thinning ability induced by the supramolecular interactions imparted by the addition of GelM to silk regenerated solution (**Figure 20**). This experiment was run at room temperature (~25°C) to match the temperature of the ink during bioprinting.

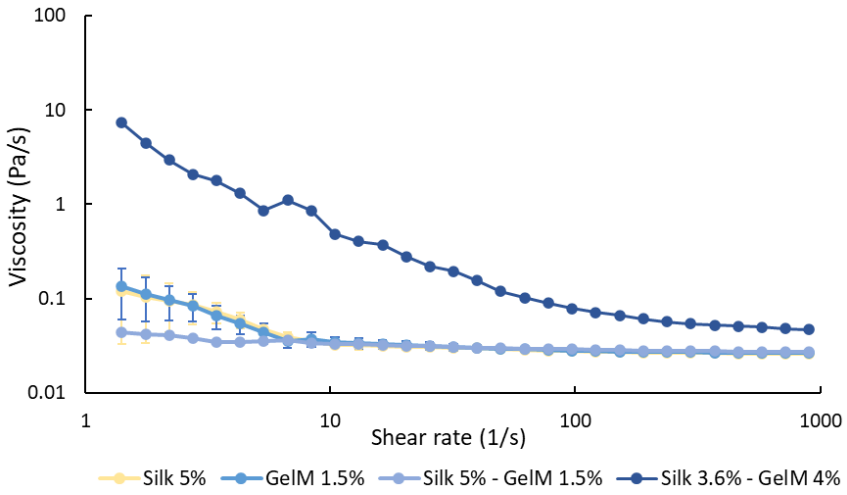

Figure 20 – Viscosity values in Pa/s for solutions made of silk, modified gelatine (GelM) and two blends of silk with GelM. Silk was boiled for 5min. The results presented are an average of four measurements (n=4) for Silk 5%, two measurements (n=2) for GelM 1.5% and Silk 5% - GelM 1.5% and one measurement (n=1) for Silk 3.6% - GelM 4%.

The viscosity at low shear-rates for the Silk 5% and GelM 1.5% solutions, within the number of samples measured, seems to be in a similar range (**Figure 20).** When these two components are mixed to yield a solution with the same final concentration of each component (*i.e.* 5% Silk and 1.5% GelM), there was no increase in viscosity (**Figure 20**). This might be explained by the low number of physical interactions between Silk 5% - GelM 1.5%, probably because there were not enough CD molecules to react with the tyrosine residues on silk's chain to drive an increase in viscosity.

Thus, a solution where the ration of Silk/GelM was inverted was tested (*i.e.* 4% GelM and 3.6% Silk). A high increase (~10x) in the viscosity of the solution at low shear rates was observed (**Figure 20**). This increase is likely due to the reversible interactions between the tyrosine residues on the silk chains and the CD on gelatine's chains.

It is also important to mention that the CD on gelatine chains might also interact with the tyrosine residues on the gelatine chains, however since the amount of Tyr in gelatine is much lower (~ 0.7% for type A, porcine skin gelatine[161]) than in silk (~5%[33]) these type of interactions are, most likely, residual.

The Silk 3.6% - GelM 4% solution blend, showed shear thinning behaviour (**Figure 20**). Shear-thinning behaviour means that there is a decrease in viscosity when the shear rate is increased, which is advantageous in bioinks used in EB. Most likely at high shear rates the reversible supramolecular interactions between CD and Tyr are broken apart, thus allowing for an ease of flow of the two polymers.

Furthermore, for EB, the viscosity of bioinks ranges between 30 mPa/s and $6x10^7$ mPa/s[139]. The value obtained for the Silk-GelM blend that showed shear-thinning behaviour: Silk 3.6% - GelM 4% (viscosity of ~10 Pa/s, **Figure 20**) is within this range. With these results, it might be interesting to investigate a ink formulation where there is a higher ratio of GelM to silk, and additionally increase the gelatine CD modification degree in order to increase the number of host-guest interactions[105].

Hydrogel photo-crosslinking

After printing, the supramolecular ink needs to be further stabilized because host-guest supramolecular interactions are physical, reversible crosslinks that result in constructs with weak mechanical properties and rapid degradation rates[100].

In this project, a photo-crosslinking method was used to stabilize the printed construct because it offers temporal and spatial control over the reaction[173]. More specifically,

riboflavin/sodium persulfate was used as a photo-initiator system, and visible light as a light source. Indeed, Heo *et al* showed that riboflavin-induced photo-crosslinking of collagen hydrogels improved mechanical properties and delayed degradation[174].

Furthermore, these components (i.e. riboflavin and sodium persulfate) can be mixed in the ink prior to printing and irradiated with visible light either during or immediately after dispensing[173]. Thus, in order to study the characteristics of different Silk - Gelatine blends photo-crosslinked constructs, photo-crosslinked gels were made using riboflavin as a photo-initiator (**Figure 21**).

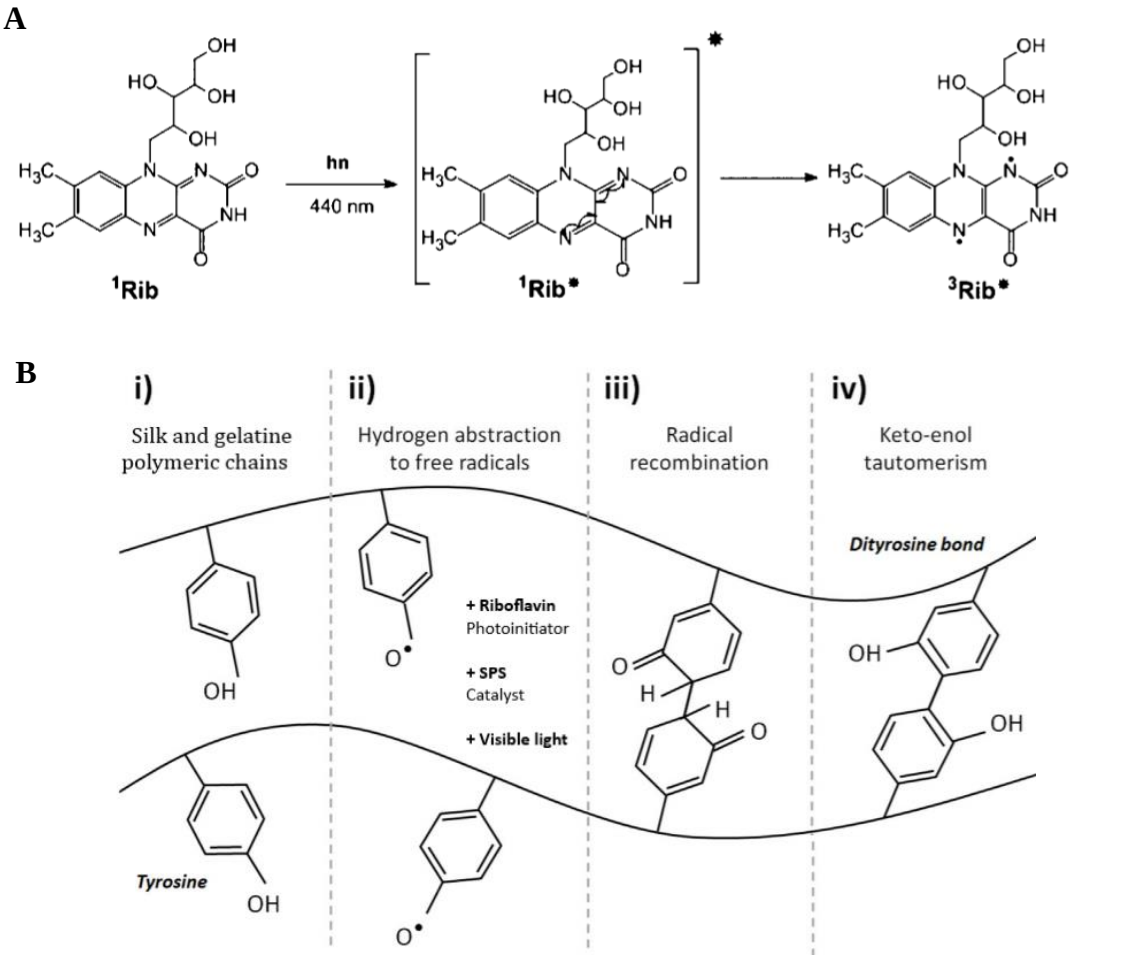

Figure 21 – Photo-crosslinking of silk and gelatine polymeric chains. ***A.*** *Formation of light induced excited states of riboflavin. Light maxima wavelength absorption of around 440 nm.* ***B.*** *Chemical mechanism for dityrosine bonding:* ***i)*** *silk and gelatine contain tyrosine residues within their peptide chains;* ***ii)*** *tyrosine has a hydroxyl group that is susceptible of being deprotonated upon interaction with free radicals formed between SPS and riboflavin upon exposure to visible light;* ***iii)*** *unbalanced terminal bonds can recombined with other unbalanced terminal bonds in adjacent chains;* ***iv)*** *the final chemical equilibrium is reached via keto-enol tautomerism when dityrosine bonds between chains are stable. Figures adapted from Cardoso et al[176] and Navarro et al[175], respectively.*

Riboflavin is a biocompatible vitamin B2 that has shown, in previous studies, minimal cytotoxicity[176]. Riboflavin can undergo reversible redox reaction by accepting/losing a pair of hydrogen atoms (reduced/oxidized) which can induce a crosslinking reaction[176].

The crosslinking mechanism starts with the excitation of riboflavin by light absorption with ʎ = 220 - 450 nm, which means that either UV or visible light can be used[162,176] (**Figure 21 - A**). Visible light was chosen for this project to avoid the potential deleterious effects of UV on embedded cells[162,174].

When riboflavin absorbs the light energy from visible light, it turns into its excited short-lived singlet state (**Figure 21**, ^{1}Rib*) before transforming into a highly reactive long-lived triplet-excited state (i.e. ^{3}Rib*)[162](**Figure 21 - A**). ^{3}Rib* can react with substrates (**Figure 21 – B i)**), in this case, it can abstract the hydrogen atom from the tyrosine hydroxyl group (-OH), yielding a free radical (-O˙) that is stabilized by the aromatic ring (**Figure 21 – B ii)**). Two of these tyrosine radicals can interact with each other (**Figure 21 – B iii)**) and form a tyrosine bond through keto-enol tautomerism[175] (**Figure 21 – B iv)**).

To determine the extent of crosslinking and swelling ability, hydrogels were characterized by sol-fraction and swelling ratio experiments. The physical properties of these hydrogels were also studied through rheological experiments.

Sol-fraction and Swelling ratio

To determine if the silk chain length influenced the degree of crosslinking and the swelling ability of the photo-crosslinked hydrogels, samples made of silk boiled for 5, 10 and 30 min were used in the sol-fraction and swelling ratio experiments.

For both the sol-fraction and the swelling experiments the photo-crosslinked hydrogels were incubated at 37°C in deionized water for 24 h. Due to the physical reversible nature of the CD-Tyr interaction and to gelatine's thermosensitivity, it is plausible that some of these interactions might break apart when the gels are incubated at 37°C and allow for some chains to leave the network. Thus, these two experiments will show mostly the effect of the chemical bonds between Tyr -Tyr residues.

Sol-fraction

The sol-fraction indicates the fraction of the polymer that is not part of the cross-linked network[91] and it was determined for crosslinked hydrogels made of Silk 5% boiled for 5,

10 and 30 min (**Figure 22**) and for Silk 5%; Silk 5% – Gel 1.5%; Silk 5% - GelM 1.5% and of Silk 5% - GelM 2.5% hydrogels using silk boiled for 5 min (**Figure 23**).

The Silk 5% hydrogels boiled for 5 min had a sol fraction of about 33.9 ± 2.3% which is higher than that obtained for the Silk 5% hydrogels boiled for 10 and 30 min, with a sol-fraction of 26.1 ± 4.9% and 12.5 ± 1.2%, respectively (**Figure 22**). These results indicate that polymer chain length might influence the crosslinking efficiency of the final photo-crosslinked hydrogels since the longer the silk chain length the higher the sol-fraction. This might be explained by the amount of Tyr in relation to the chain length hence, for longer chain sizes the ratio of tyrosine residues is lower thus resulting in a lower degree of chemical crosslinking. However, the use of longer polymeric chains can be advantageous because it is accompanied by an increase in viscosity[177].

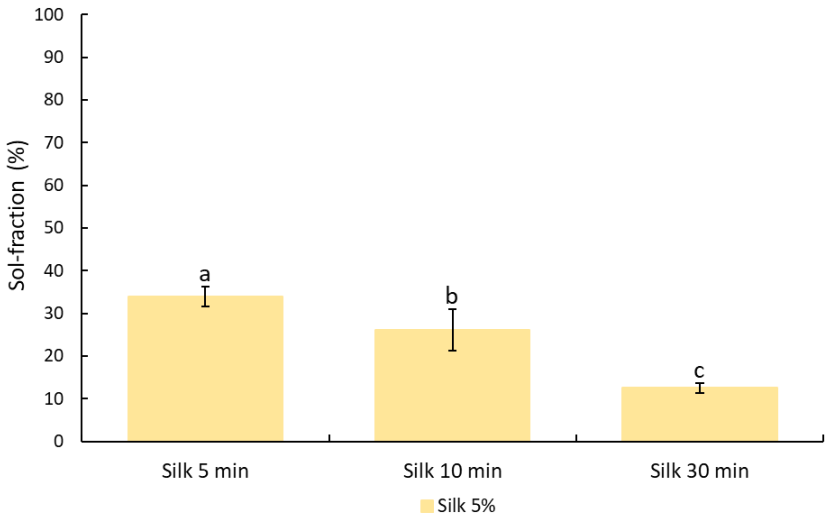

Figure 22 –Sol-fraction (average ± sd) of the crosslinked hydrogels made of silk boiled for 5, 10 and 30 min. The results presented are an average of at least three technical replicates (n≥3). Bars with different letters differ p<0.05.

The sol-fraction of Silk 5% hydrogels boiled for 5 min was of 33.9 ± 2.3%, which was lower than for Silk 5% - GelM 1.5% and 2.5% hydrogels with a sol fraction of 44.0 ± 3.1 and 48.0 ± 2.0%, respectively (**Figure 23**). Hence, the addition of GelM to silk increases the sol-fraction and decreases the cross-linking effectiveness. This can be due to the following reasons: firstly, there are less Tyr available for the photo-crosslinking of the silk chains because they are sterically hindered by their inclusion in CD cavity. As such, less Tyr are available for permanent crosslinking between tyrosine residues both on silk and on gelatine polymeric chains. Additionally, as mentioned before, gelatine's thermosensitivity might allow for some physically crosslinked chains to leave the

network when incubated at 37°C. So, the results might only mirror the extent of chemical crosslinking.

Furthermore, the addition of 1.5% of Gel to Silk 5% results in a lower sol-fraction, 10.9 ± 4.3%, than Silk 5% (boiled for 5 min) and Silk 5% - GelM hydrogels (**Figure 23**). This indicates that the addition of Gel increases the crosslinking effectiveness which might be explained by 1. the addition of gelatine polymers with Tyr residues may increase the chemical crosslinking when comparing to the Silk 5% (boiled for 5 min) hydrogels. Moreover, the small size of gelatine chains could favour its entrapment inside the silk/gel cross-linked network, as has been previously described[80]; and 2. Since Silk - Gel chains only have chemical irreversible crosslinks, the amount of polymer that might leave the network at 37°C is much lower when comparing to the Silk - GelM hydrogels.

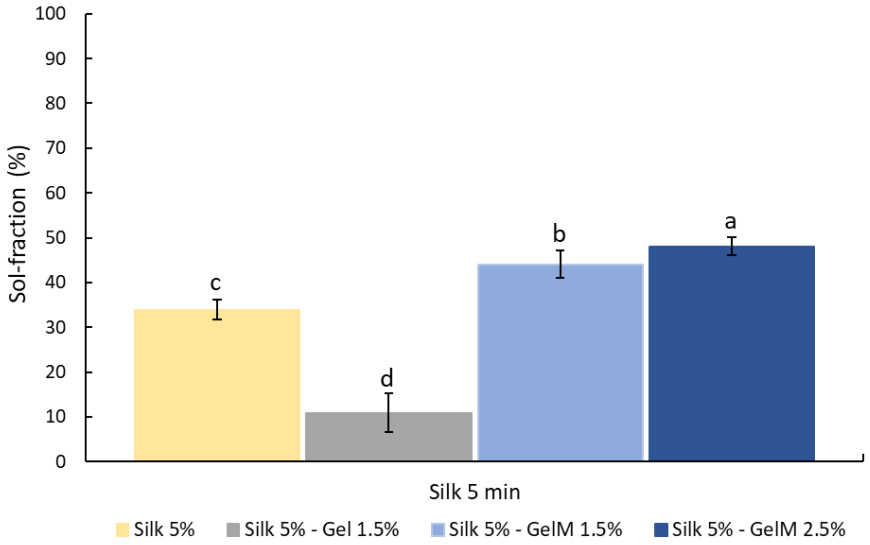

Figure 23 - Sol-fraction (average ± sd) of the crosslinked hydrogels made of silk and a blend of silk with non-modified (Gel) and modified (GelM) gelatine. Silk was boiled for 5 min. The results presented are an average of at least three technical replicates (n≥3). Bars with different letters differ p<0.05.

The overall trend for the sol-fraction in decreasing order is as follows: Silk 5% - GelM 2.5% > Silk 5% - GelM 1.5% > Silk 5% (5 min > 10 min > 30 min) > Silk 5% - Gel 1.5%. In spite the variation observed among the sol-fraction of the different hydrogels tested, all blends showed a good crosslinking efficiency since all hydrogels had a sol-fraction value below 50%.

Swelling ratio

Silk-Gelatine hydrogels were characterized by swelling measurements performed at 37°C. The swelling ratio represents the increase in weight due to water absorption[91],

which is important for cell viability and proliferation[137]. The swelling ability of an hydrogel is influenced by several factors, such as the molecular weight of the polymer chains; the polymer concentration and the extent of crosslinking[91]. The values obtained for the swelling ratio of the different hydrogel made of Silk 5% boiled for 5, 10 and 30 min are shown in **Figure 24** and for the Silk 5%; Silk 5% – Gel 1.5%; Silk 5% - GelM 1.5% and of Silk 5% - GelM 2.5% hydrogels using silk boiled for 5 min are shown in **Figure 25**.

The swelling ratio was dependent on the silks chain length because the swelling ratio of the photo-crosslinked hydrogel with silk boiled for 30 min (2.2 ± 0.4) is significantly lower when comparing to silk boiled for 5 min (11.8 ± 1.3) and 10 min (13.4 ± 2.4) (**Figure 24**). This can be explained by the closer proximity between crosslinks as the polymer chain length decreases, resulting in smaller mesh size, hence less swelling can occur. However, there is not a significant difference between swelling ratio of the Silk hydrogels made of silk boiled for 5 and 10 min. This can probably be explained by the lower differences in silk MW of silk 5 and 10 min when comparing to silk 30 min due to the variations of their boiling times.

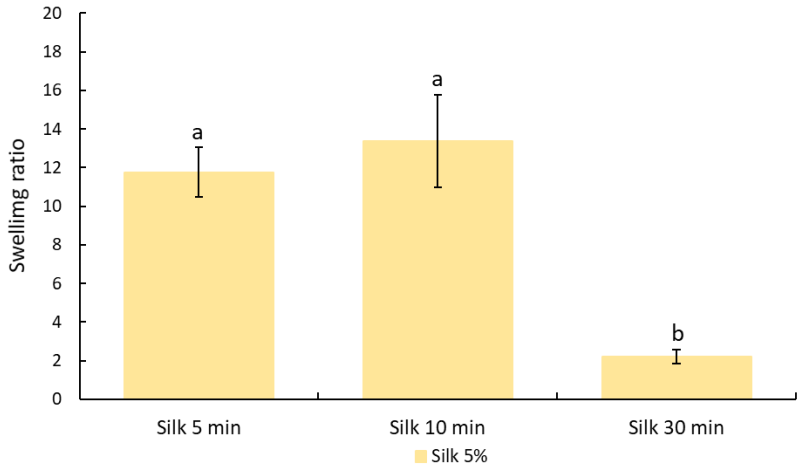

Figure 24 - Bar-plot of the swelling ratio (average ± sd) of the crosslinked hydrogels made of silk boiled for 5, 10 and 30 min. The results presented are an average of at least three technical replicates (n≥3). Bars with different letters differ p<0.05.

A low swelling ratio, as observed for silk 30 min, would be an indication of higher crosslink density and low mesh size which might hinder nutrient diffusion and thus potentially have a negative impact on cell viability[137,178]. Thus, hydrogels made from silk boiled for shorter periods (5 min or 10 min) seem to be the most promising in terms of cellular viability.

There are however conflicting results; while Park *et al* saw a detrimental effect on chondrogenic differentiation in hydrogels with lower swelling ratios[91], Lee *et al* reported enhanced osteoblast differentiation in alginate hydrogels with smaller mesh sizes and higher mechanical rigidity[179]. Hence it seems that other parameters need to be taken into account such as the desired type of tissue, the mechanical properties of the hydrogel and its degradation rate[180].

The swelling ratio for the Silk 5% - GelM 1.5% and 2.5% is of 10.8 ± 1.1 and 11.5 ± 1.0, respectively (**Figure 25**). Therefore, the addition of GelM to silk does not affect the swelling ratio when compared to the Silk 5% (boiled for 5 min) hydrogels, these results might be explained by the reversible nature of the CD-Tyr interactions which can be rearranged to accommodate water molecules. Additionally, the increase in GelM concentration (from 1.5% to 2.5%) did not have any effect on the swelling ratio. Which might be due to the relatively small increase of GelM (1%**)** and the reversible nature of the CD-Tyr bonds.

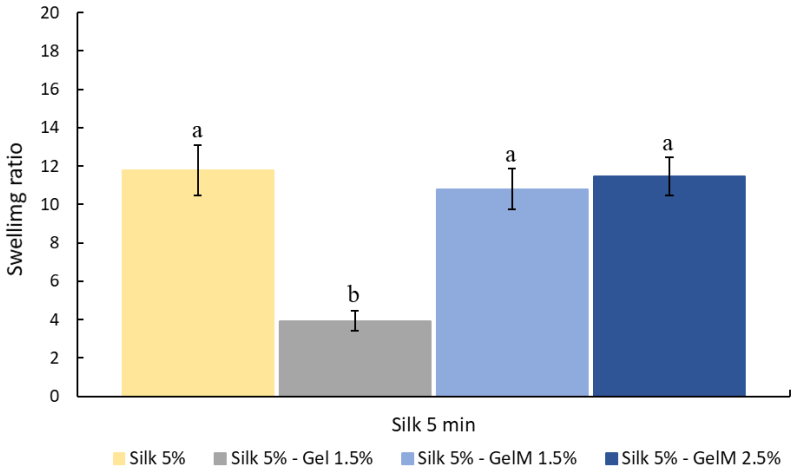

Figure 25 - Bar-plot of the swelling ratio (average ± sd) of the crosslinked hydrogels made of silk and a blend of silk with non-modified (Gel) and modified (GelM) gelatine. Silk was boiled for 5. The results presented are an average of at least three technical replicates (n≥3). Bars with different letters differ p<0.05.

Silk 5% - Gel 1.5% hydrogels with a swelling ratio of 3.9 ± 0.5 showed very low swelling in comparison to the Silk 5% (boiled for 5 min) hydrogels (**Figure 25**). This means that the addition of Gel creates a hydrogel with a smaller water absorption capacity, which indicates a smaller mesh size. This smaller mesh size could be explained by the presence of irreversible Tyr-Tyr bonds between the smaller gelatine chains with the silk chains. It can be hypothesized that the differences in sizes of gelatine (50-100 kDa[181]) and silk

chains (boiled for 5 min) create tighter bonds, similar to the ones present in the Silk 5% (30 min) hydrogels (**Figure 24**).

Rheological characterization: Silk – Gelatine photo-crosslinked hydrogels

The following rheological characterization of the photo-crosslinked hydrogels were performed using silk boiled for 5 min. Because host-guest supramolecular interactions are reversible dynamic bonds, it is expected that the Silk-GelM hydrogels formed show shear-thinning and recovery properties[100]. Furthermore, since these physical bonds can be easily broken apart by mechanical forces, the following rheological data will mainly mirror the contribution of the chemical irreversible bonds present in the hydrogels. The G' (storage modulus) and the G'' (loss modulus), characterize the elastic and viscous nature of the samples, respectively.

Amplitude Sweep

Amplitude sweep measurements were performed in a range of 0.5-600 strain and constant frequency to determine the LVR of the photo-crosslinked hydrogels. The LVR of the material is the region where its viscoelastic properties are independent of imposed stress or strain levels. This region indicates the range at which rheological tests can be run without damaging the structure of the sample[182]. It also gives an indication of the hydrogel's ability to prevent sedimentation[80] because the LVR determines the limit (in this case the strain) at which the structure of the construct gets deformed (*i.e.* yield stress).

The strain sweep for the Silk 5% and the Silk 5% - GelM 1.5% photo-crosslinked hydrogel is shown in **Figure 26.**

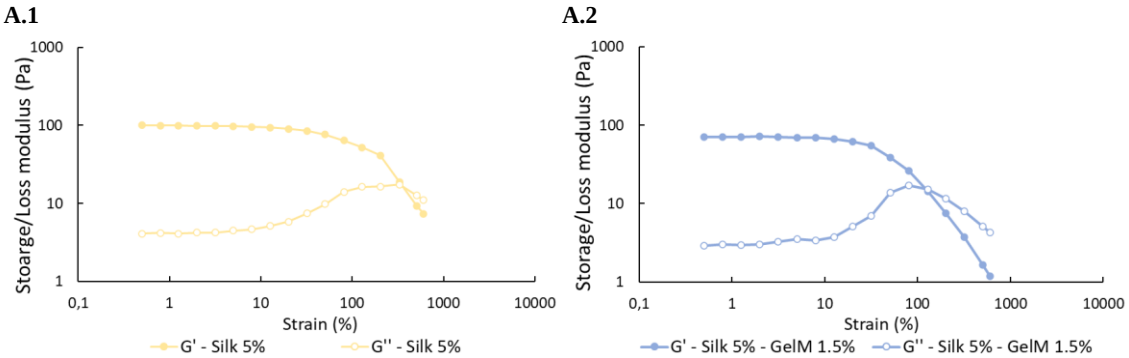

*Figure 26 – Amplitude sweep for **A.1** 5% silk hydrogel, boiled for 5 min, and for **A.2** 5% silk and 1.5% GelM hydrogel. Only one measurement was taken for each sample type.*

Both hydrogels show linear behaviour of G' up to ~20% strain and a solid elastic gel-like structure because G' > G'' (**Figure 26**). Furthermore, the LVR for the Silk 5% hydrogels

is ≤ than 20% strain and for the Silk 5% - GelM 1.5% is ≤ than ~13% strain (determined by ± 10% G' deviation from the first measurement). These strain limits of the LVR are also called yield points.

Silk 5% - GelM 1.5% hydrogels (**Figure 26 – A.2**) show a steeper decrease of the G' at increasing strain levels in comparison to the 5% Silk hydrogels (**Figure 26 – A.1**). Furthermore, both hydrogels undergo solid to fluid transition (*i.e.* flow point), thus becoming a viscous fluid like structure (G'' > G'), at ~129% strain and ~330% strain for Silk 5% - GelM 1.5% and Silk 5% hydrogel, respectively.

The decrease of G' and inversion of the loss and storage moduli indicates structure breakdown due to large deformations[166]. Thus, it seems that the addition of GelM to Silk makes the resulting hydrogel structure more readily deformable (**Figure 26**). This is likely due to the additional presence of reversible physical bonds that will contribute in two ways for this result: 1. physical bonds are more readily broken[96] and 2. the presence of CD decreases the number of Tyr available to undergo chemical, irreversible crosslinking.

Additionally, the difference between the yield point and the flow point (when G'' > G') can be used to infer about the materials flexibility or brittleness. If the transition is very abrupt that would mean that the hydrogels were very brittle. However, the two tested hydrogels appear to be flexible (**Figure 26**).

Frequency Sweep

A frequency sweep provides a relative ranking of the elastic and viscous properties of a material at increasing frequencies (rate of deformation) and under constant strain and temperature. The high frequency region corresponds to short-term behaviour while the low frequency region mimics long-term behaviour[183].

The frequency sweep measurements were performed at a strain (1%) within the LVR determined previously (**Figure 26**) and at 25°C. The frequency dependence of moduli and the phase angle (tan δ) of the Silk 5%; Silk 5% – Gel 1.5%; Silk 5% - GelM 1.5% and of Silk 5% - GelM 2.5% hydrogels is presented in **Figure 27.**

The G' was independent of frequency for all hydrogels at low frequencies (**Figure 27 – A. 1 and 2**). Furthermore, at lower frequencies, G' was higher than G'' for all hydrogels,

meaning that the elastic response is dominant when at rest. Therefore, all studied hydrogels appear to be solid-like at low frequencies and are, consequently, crosslinked[184].

G' is an indicator of an hydrogels ability to store deformation energy in an elastic manner, a high G' value would indicate a high crosslinking density and strength or mechanical rigidity of the hydrogel[185]. The G' varied between gels in the following order: Silk 5% - Gel 1.5% > Silk 5% - GelM 2.5% > Silk 5% - GelM 1.5% > Silk 5% (**Figure 27 – A.1 and 2**). Thus, the results indicate that gelatine, especially the non-modified, creates more resilient hydrogels that have a higher crosslinking density.

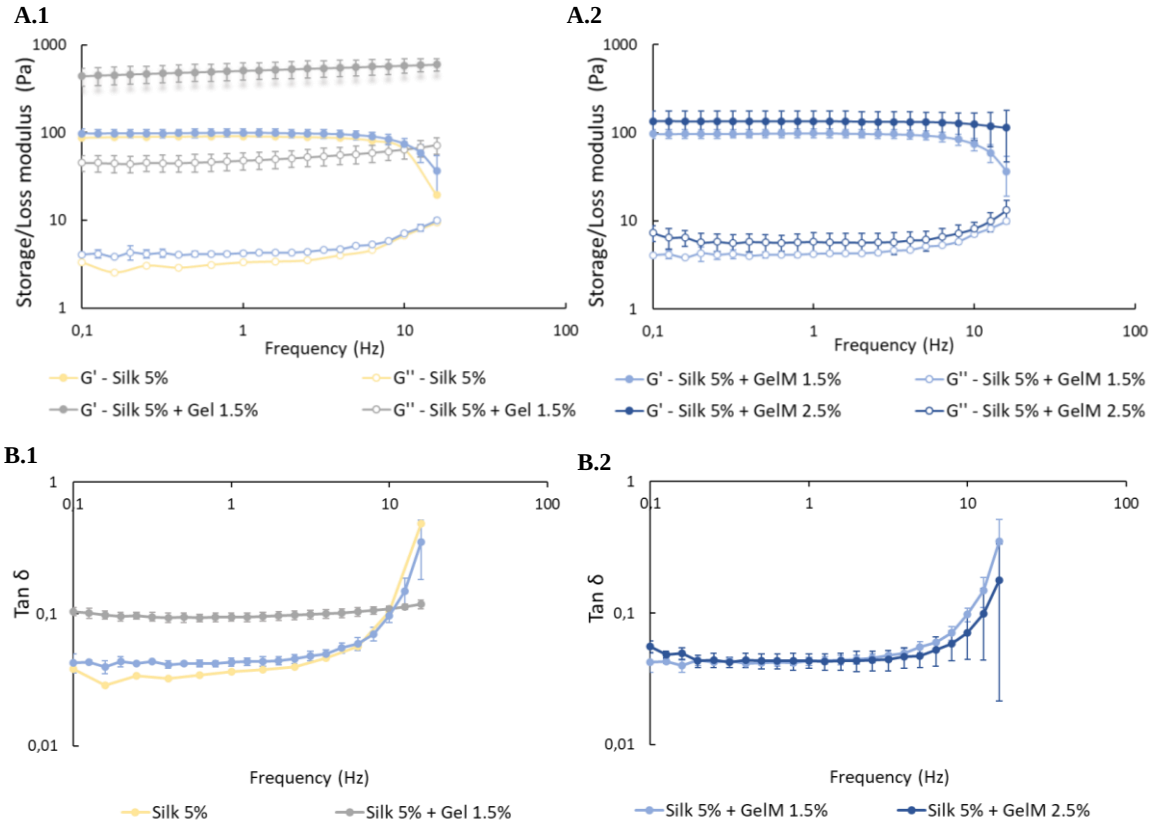

Figure 27 – Frequency sweep of hydrogels made of silk boiled for 5 min alone or of a mixture of silk and modified and unmodified gelatine. ***A.*** *The storage (G') and loss (G'') modulus of the different gels and* ***B.*** *The tan delta (G''/G') of the different hydrogels. The results shown are from three different hydrogels (n=3) except for the silk 5% hydrogel for which only one gel was measured (n =1).*

At increasing frequencies, the G' of the Silk 5% - Gel 1.5% hydrogels stays constant, probably due to the lower mobility of the chains between the crosslinks due to a small mesh sized. While G' decreased for the other gels, for Silk 5% hydrogels this might be due to the high mobility of a sparsely crosslinked high-molecular weight polymer mesh.

For the Silk 5% - GelM 1.5 and 2.5% hydrogels the decrease in G' is most likely due to the break of the physical Tyr-CD bonds (**Figure 27 – A.1 and 2**).

Furthermore, the decrease of G' occurs at higher frequencies with the increase of GelM to Silk ratio (**Figure 27 – A.2**). This trend might indicate that the addition of GelM at higher concentrations (more than 2.5%) might be a good strategy to increase the hydrogels strength without affecting its water adsorption capacity, and consequently, cell viability.

The tan δ indicates the extent of elasticity of the hydrogels and it can be calculated through the following ratio: $\tan\delta = \frac{G''}{G'}$. If tan δ > 1 it means that the material behaves as a viscous fluid, while if tan δ < 1 the material behaves like an elastic solid.

From **Figure 27 – B.1 and 2**, it can be concluded that all hydrogels have a tan δ < 1, and that the Silk 5% - Gel 1.5% hydrogels store less deformation energy in an elastic way. This indicates that there are more polymeric chains with free mobility and thus, unlinked. This could mean, as mentioned before, that gelatine chains might be entrapment inside the silk/gel cross-linked network[80].

However, Silk 5% - Gel 1.5% hydrogels maintain their structure for a longer range of frequencies in comparison to the other hydrogel formulations (**Figure 27 – B.1 and 2)**. This might be due to the presence of more irreversible chemical bonds (Tyr-Tyr) between the gelatine and silk chain.

Shear recovery

To determine if the photo-crosslinked hydrogels were able to regain their shape after deformation, they were subjected to cycles of large amplitude oscillatory strain followed by low oscillatory strain (**Figure 28**). The strain sweeps previously performed, **Figure 26**, were used to determine a low (1%) and a high (500%) strain for the recovery experiments.

Under cyclic deformation, all hydrogels showed a clear decline in G' modulus at high strain conditions and rapid recovery of initial mechanics at low strain. These results show that the hydrogels are capable of near-immediate recovery following deformation (**Figure 28**). Furthermore, all hydrogel compositions except the Silk 5% hydrogels (**Figure 28 – A.1**) showed a gel-sol transition on the onset of high strain, which is visible by the overlap

of the G'' modulus over the G' modulus at high strains (**Figure 28 A.2-4)** and by the tan δ >1 values **(Figure 28 – B.1)**.

The reason for the absence of the G'' and G' overlap at high strain for Silk 5% hydrogels might be the fact that they are chemically crosslinked. These hydrogels can, however, withstand high strain forces, probably due to the high molecular weight of the silk polymer and lower crosslinking density which allows for higher mobility (*i.e.* reducing molecular entanglement) without structural breakdown[184].

On the other hand, the G'' and G' overlap for Silk 5% – Gel 1.5% hydrogels at high strains, might be due to the presence of physical interactions which are broken at high

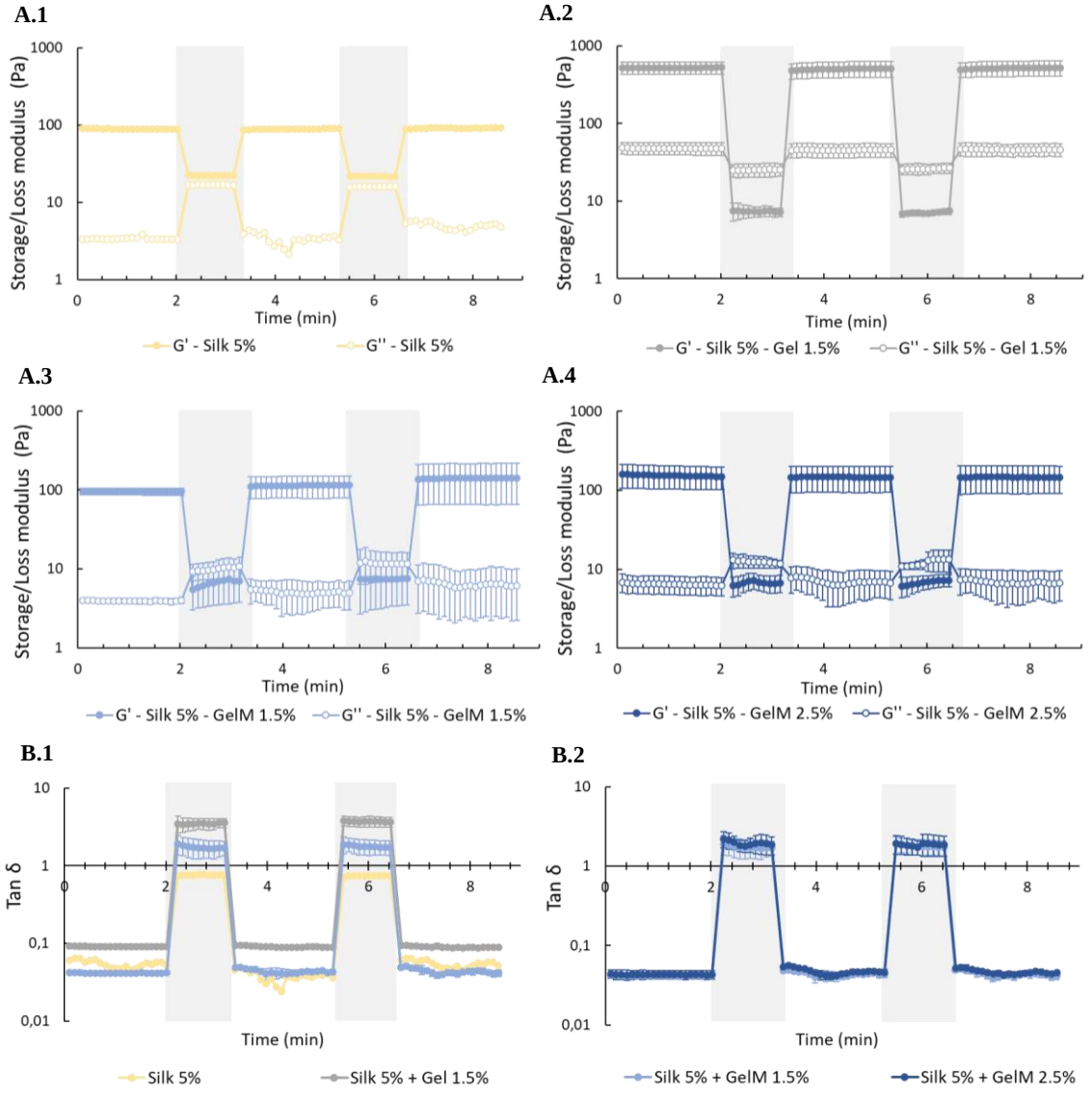

Figure 28 – Cyclic deformation of crosslinked hydrogels made of 5% silk, 5% silk and 1.5% Gel or 1.5% GelM or 2.5% GelM at 1% (unshaded areas) and 500% (shaded areas) strain. ***A.*** *Values of the storage G' and loss modulus G'' for each type of hydrogel and* ***B.*** *Values of tan delta for all the diferent types of hydrogels. The results shown are from three different gels (n=3) except for the silk 5% gel for which only one hydrogel was measured (n =1).*

strain and reassemble at low strain. Indeed, Silk and Gel polymers might form semi- or interpenetrating polymer networks upon gelatine gelation and Tyr-Tyr chemical crosslinking. For Silk 5% – GelM 1.5 and 2.5% hydrogels, although they might also have these types of physical interaction the one that contributes the most for this overlap will most likely be the CD-Tyr supramolecular interaction. The fact that at a high strain the G'' dominates over the G' on the mixed blends raises the possibility of bioprinting the photo-crosslinked hydrogel[100].

Furthermore, according to the tan δ values it seems that the addition of non-modified gelatine leads to an overall more viscous hydrogel (**Figure 28 – B.1**). These results are in accordance with the results obtained from the frequency sweep (**Figure 27)**.

Average mesh size, crosslinking density, and average molecular weight of the polymer chain between neighbouring crosslinks of the hydrogels

The G' and G'' of the hydrogels presented on **Table 4** were calculated from the frequency sweep results for frequencies comprised between 0.1-1 Hz. The results show that the G' increases with the addition of gelatine, and that the addition of Gel results in a higher increase than GelM. Additionally, the higher the GelM final concentration the higher is the G'. Hydrogels arranged from decreasing G' are: Silk - Gel 1.5% > Silk - GelM 2.5% > Silk - GelM 1.5% > Silk. The G'' also follows this order.

Generally, hydrogels with a higher G' tend to have a higher resilience to deformation[166,184] Thus, in this case, hydrogels made of Silk 5% - Gel 1.5% seem to be the ones that show the most resistance to deformative forces. These results agree with the frequency sweep analysis (**Figure 27**), where these hydrogels seemed to retain their shape for a higher range of frequencies.

Table 4 - Storage (G') and loss (G'') modulus, the plateau value for G' (G_e), the average mesh size, the average crosslinking densities (n_e) and the average molecular weights of the polymer chains between neighbouring crosslinks (Mc) of of silk boiled for 5 min, Silk - Gel and Silk - GelM crosslinked hydrogels (average ± sd) determined based on the rheological frequency sweep analysis. The results shown are from three different gels (n=3) except for the silk 5% gel for which only one hydrogel was measured (n =1).

Gel type	G' Pa	G'' Pa	G* Pa	G_e Pa	Mesh size nm	n_e mol/m^3	M_c kg/mol
Silk 5%	89	3	89	89	35.9	0.036	1386
Silk 5% - Gel 1.5%	474 ± 105	46 ± 10	476 ± 106	576 ± 112	20.8 ± 1.7	0.232 ± 0.045	225 ± 50
Silk 5% - GelM 1.5%	98 ± 11	4 ± 0.3	98 ± 11	98 ± 11	34.9 ± 1.4	0.040 ± 0.004	1274 ± 150
Silk 5% - GelM 2.5%	134 ± 34	6 ± 1	134 ± 34	134 ± 34	31.7 ± 2.5	0.054 ± 0.014	977 ± 223

The average mesh size, n_e and M_c were calculated, and the results are presented in **Table 4**. The n_e follows the same trend as the G', thus the decrescent order of crosslinking density is as follows: Silk 5% - Gel 1.5% > Silk 5% - GelM 2.5% > Silk 5% - GelM 1.5% > Silk 5%.

As it would be expected, the higher the n_e, the lower the mesh size and the M_c, thus the decrescent order of these parameters is the following: Silk > Silk - GelM 1.5% > Silk - GelM 2.5% > Silk - Gel 1.5%.

This means that the addition of gelatine (either Gel or GelM) increases the number of crosslinks and decreases the pore sizes of the mesh. The addition of Gel, when comparing to GelM, accentuates this trend, in fact, Silk 5% - Gel 1.5% hydrogels have a lower mesh size and a higher crosslinking density than the Silk - GelM 2.5% hydrogel that has 1% more gelatine. These results are in accordance with the results of the frequency sweep (**Figure 27 – A.1 and 2**). However, it is important to point out that due to the reversible nature of physical crosslinks, the results shown in **Table 4** will most likely mainly mirror the contribution of the chemical crosslinks.

Furthermore, even though Silk 5% - Gel 1.5% hydrogels seem to be more densely crosslinked, the values of tan δ from the frequency sweep (**Figure 27 - B**) and shear-recovery experiments (**Figure 28 - B**) show that the resultant hydrogels are less elastic. This might mean that, although it has a tighter mesh, the interactions between the chains are weaker such that they can dissipate more deformation energy.

Lastly, it should be noted that a tightly crosslinked mesh might be problematic in terms of cell viability, since cells require space to grow and proliferate as well as free exchange of nutrients and oxygen[178].

Printability

To determine if a Silk - GelM blend could be used in extrusion bioprinting some preliminary tests were run. Several blends of S-β-CD functionalized gelatine and silk were prepared.

Mixtures with a final concentration of 5% Silk - GelM 1.5, 2.5 and 4.5% were tried out, however the solutions were too liquid to be printed (extruded as droplets) (**Figure 29 - A**). Thus, the viscosity of the mixture was increased though the addition of 3.5% Gel. This composition allowed for the printing of a 1-layer and a 3-layer structure using a 27G and a 25G cylindrical nozzle, respectively (**Figure 29 – B and C**). However, for the 3-

layer structure the different layers seem to blend into each other. This problem can be surpassed with the photo-crosslinking of each layer as it is extruded.

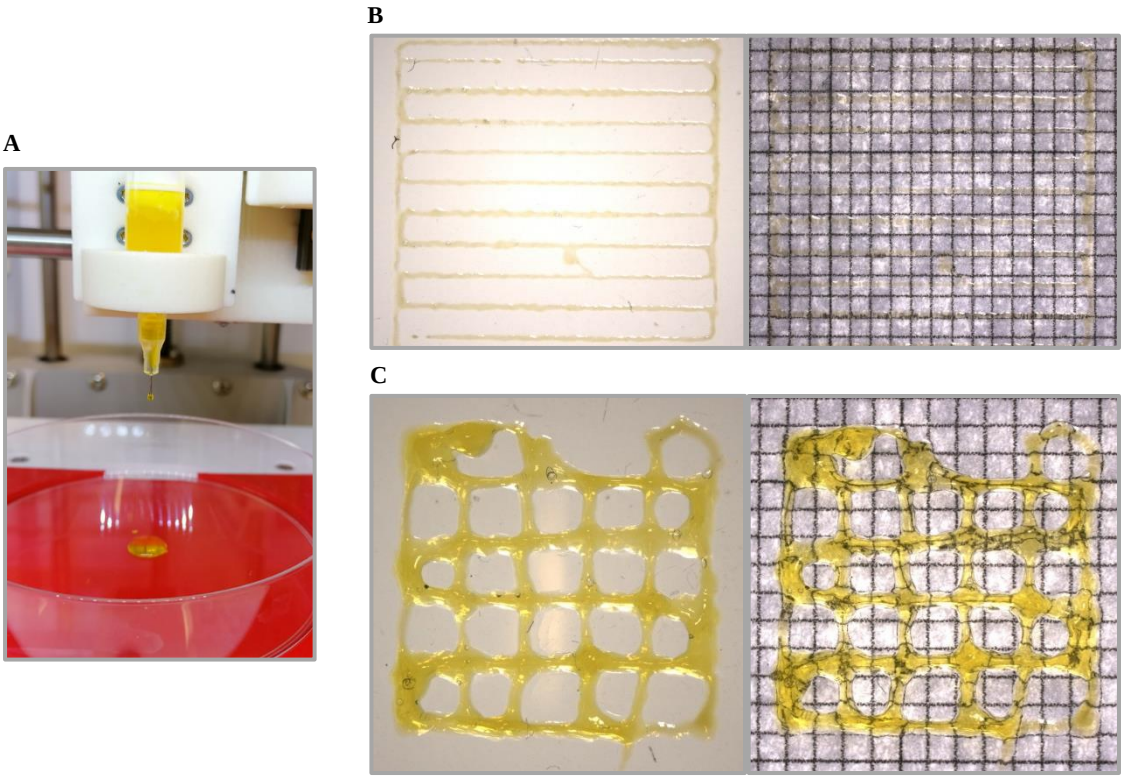

*Figure 29 – **A.** Extrusion of a 5% Silk - GelM 1.5% solution as droplets; Extrusion bioprinting with 5% Silk, GelM 4.5% and Gel 3.5% of: **B.** 1-layer construct using a 27G cylindrical nozzle and **C.** 3-layer construct using a 25G cylindrical nozzle. Pictures taken with graph paper.*

Conclusions

In summary, the functionalization of gelatine with succinyl-β-cyclodextrin was successfully achieved. The addition of GelM to silk in higher ratios increased the viscosity of the final solution which is thought to be due to Tyr-CD host-guest interaction. All hydrogel compositions tested in this project were effectively photo-crosslinked using riboflavin as a photo-initiator.

Silk - GelM photo-crosslinked hydrogels have a combination of chemical and physical crosslinking and seem to be less chemically crosslinked than all other tested compositions. They show a higher swelling ability and are more readily deformable than Silk - Gel photo-crosslinked hydrogels but, are more elastic (more flexible) than all other tested compositions.

Silk - Gel photo-crosslinked hydrogels are more chemically crosslinked, show a lower swelling ability, are more resistant to deformation, nevertheless, resulted in less elastic hydrogels (less flexible) than all other tested compositions.

All photo-crosslinked hydrogels could recover their initial mechanics after a period of high strain, and the addition of gelatine (either Gel or GelM) imparted shear-thinning characteristics to the hydrogels, which can be advantageous for bioprinting purposes. From preliminary printability testing it seems that the developed formulations are suitable to be used as biomaterial inks.

Future Perspectives

All rheological tests performed should be completed on all blends and repeated in triplicate to guarantee the robustness of the results.

A higher ratio of GelM to Silk blend or the use of GelM with a higher degree of modification should be investigated since the solution with a higher GelM to silk ratio showed an increase in viscosity when compared to the other tested blends. Furthermore, to better understand how the Tyr-CD interactions drives the gelation of the Silk - GelM blend an *in-situ* gelation test could be performed with a rheometer.

An evaluation of the cellular behaviour of the photo-crosslinked hydrogels should be investigated to determine the cytocompatibility of the Silk - GelM blend. To this end, Live-Dead staining and DNA quantification could be performed to evaluate cellular viability and proliferation.

Lastly, the bioprinting of photo-crosslinked Silk – Gelatine hydrogels should also be explored.

References

1. Mason, C. & Dunnill, P. A brief definition of regenerative medicine. *Regen. Med.* **3**, 1–5 (2008).

2. Greenwood, H. L. *et al.* Regenerative medicine: New opportunities for developing countries. *Int. J. Biotechnol.* **8**, 60–77 (2006).

3. Malda, J. *et al.* 25th anniversary article: Engineering hydrogels for biofabrication. *Adv. Mater.* **25**, 5011–5028 (2013).

4. Chan, B. P. & Leong, K. W. Scaffolding in tissue engineering: General approaches and tissue-specific considerations. *Eur. Spine J.* **17**, S467–S479 (2008).

5. Seliktar, D. Designing cell-compatible hydrogels for biomedical applications. *Science.* **336**, 1124–1128 (2012).

6. Cushing, M. C. & Anseth, K. S. Hydrogel cell cultures. *Science.* **316**, 1133–1134 (2007).

7. Skardal, A. *et al.* A hydrogel bioink toolkit for mimicking native tissue biochemical and mechanical properties in bioprinted tissue constructs. *Acta Biomater.* **25**, 24–34 (2015).

8. Tibbitt, M. W. & Anseth, K. S. Hydrogels as extracellular matrix mimics for 3D cell culture. *Biotechnol. Bioeng.* **103**, 655–663 (2009).

9. DeForest, C. A. & Anseth, K. S. Advances in bioactive hydrogels to probe and direct cell fate. *Annu. Rev. Chem. Biomol. Eng.* **3**, 421–444 (2012).

10. Lee, K. Y. & Mooney, D. J. Hydrogels for tissue engineering. *Chem. Rev.* **101**, 1869–1879 (2001).

11. Chao, P.-H. G. *et al.* Silk hydrogel for cartilage tissue engineering. *J. Biomed. Mater. Res. Part B Appl. Biomater.* **95B**, 84–90 (2010).

12. Liu, C., Zhang, Z., Liu, X., Ni, X. & Li, J. Gelatin-based hydrogels with β-cyclodextrin as a dual functional component for enhanced drug loading and controlled release. *RSC Adv.* **3**, 25041–25049 (2013).

13. Pepelanova, I., Kruppa, K., Scheper, T. & Lavrentieva, A. Gelatin-methacryloyl (GelMA) Hydrogels with defined degree of functionalization as a versatile toolkit for 3D cell culture and extrusion bioprinting. *Bioengineering* **5**, 55 (2018).

14. Gasperini, L., Mano, J. F. & Reis, R. L. Natural polymers for the microencapsulation of cells. *J. R. Soc. Interface* **11**, 20140817 (2014).

15. Antoine, E. E., Vlachos, P. P. & Rylander, M. N. Review of collagen I hydrogels for bioengineered tissue microenvironments: Characterization of mechanics, structure, and transport. *Tissue Eng. - Part B Rev.* **20**, 683–696 (2014).

16. Zhang, Y., Yu, Y. & Ozbolat, I. T. Direct bioprinting of vessel-like tubular microfluidic channels. *J. Nanotechnol. Eng. Med.* **4**, 020902 (2013).

17. Piluso, S. *et al.* Hyaluronic acid-based hydrogels crosslinked by copper-catalyzed azide-alkyne cycloaddition with tailorable mechanical properties. *Int. J. Artif. Organs* **34**, 192–197 (2011).

18. Larrañeta, E. *et al.* Synthesis and characterization of hyaluronic acid hydrogels crosslinked using a solvent-free process for potential biomedical applications. *Carbohydr. Polym.* **181**, 1194–1205 (2018).

19. Pauly, H. M., Place, L. W., Haut Donahue, T. L. & Kipper, M. J. Mechanical properties and cell compatibility of agarose hydrogels containing proteoglycan mimetic graft copolymers. *Biomacromolecules* **18**, 2220–2229 (2017).

20. Catoira, M. C., Fusaro, L., Di Francesco, D., Ramella, M. & Boccafoschi, F. Overview of natural hydrogels for regenerative medicine applications. *J. Mater. Sci. Mater. Med.* **30**, 115 (2019).

21. Yu, J. *et al.* The effect of injected RGD modified alginate on angiogenesis and left ventricular function in a chronic rat infarct model. *Biomaterials* **30**, 751–756 (2009).

22. Tang, S., Yang, W. & Mao, X. Agarose/collagen composite scaffold as an anti-adhesive sheet. *Biomed. Mater.* **2**, S129–S134 (2007).

23. Spiller, K. L., Maher, S. A. & Lowman, A. M. Hydrogels for the repair of articular cartilage defects. *Tissue Eng. - Part B Rev.* **17**, 281–299 (2011).

24. Fan, C. & Wang, D. A. Effects of permeability and living space on cell fate and neo-tissue development in hydrogel-based scaffolds: A study with cartilaginous model. *Macromol. Biosci.* **15**, 535–545 (2015).

25. Khetan, S. *et al.* Degradation-mediated cellular traction directs stem cell fate in

covalently crosslinked three-dimensional hydrogels. *Nat. Mater.* **12**, 458–465 (2013).

26. Altman, G. H. *et al.* Silk-based biomaterials. *Biomaterials* **24**, 401–416 (2003).

27. Rockwood, D. N. *et al.* Materials fabrication from *Bombyx mori* silk fibroin. *Nat. Protoc.* **6**, 1612–1631 (2011).

28. Meinel, L. *et al.* The inflammatory responses to silk films in vitro and in vivo. *Biomaterials* **26**, 147–155 (2005).

29. Holland, C., Numata, K., Rnjak-Kovacina, J. & Seib, F. P. The biomedical use of silk: Past, present, future. *Adv. Healthc. Mater.* **8**, 1800465 (2019).

30. Lewis, R. Unraveling the weave of spider silk. *Bioscience* **46**, 636–638 (1996).

31. Chawla, S., Midha, S., Sharma, A. & Ghosh, S. Silk-based bioinks for 3D bioprinting. *Adv. Healthc. Mater.* **7**, 1–23 (2018).

32. Inoue, S. *et al.* Silk fibroin of Bombyx mori is secreted, assembling a high molecular mass elementary unit consisting of H-chain, L-chain, and P25, with a 6:6:1 molar ratio. *J. Biol. Chem.* **275**, 40517–40528 (2000).

33. Marsh, R. E., Corey, R. B. & Pauling, L. An investigation of the structure of silk fibroin. *BBA - Biochim. Biophys. Acta* **16**, 1–34 (1955).

34. Charu Vepari; David L. Kaplan. Silk as biomaterial. *Prog. Polym. Sci.* **100**, 130–134 (2007).

35. Shi, W. *et al.* Structurally and functionally optimized silk-fibroin–gelatin scaffold using 3D printing to repair cartilage injury in vitro and in vivo. *Adv. Mater.* **29**, 1–7 (2017).

36. Koh, L. D. *et al.* Structures, mechanical properties and applications of silk fibroin materials. *Prog. Polym. Sci.* **46**, 86–110 (2015).

37. Zhou, C. Z. Fine organization of *Bombyx mori* fibroin heavy chain gene. *Nucleic Acids Res.* **28**, 2413–2419 (2000).

38. Kundu, B., Rajkhowa, R., Kundu, S. C. & Wang, X. Silk fibroin biomaterials for tissue regenerations. *Adv. Drug Deliv. Rev.* **65**, 457–470 (2013).

39. Foo, C. W. P. *et al.* Role of pH and charge on silk protein assembly in insects and spiders. *Appl. Phys. A Mater. Sci. Process.* **82**, 223–233 (2006).

40. Lefèvre, T., Rousseau, M. E. & Pézolet, M. Protein secondary structure and orientation in silk as revealed by Raman spectromicroscopy. *Biophys. J.* **92**, 2885–2895 (2007).

41. Takahashi, Y., Gehoh, M. & Yuzuriha, K. Structure refinement and diffuse streak scattering of silk (*Bombyx mori*). *Int. J. Biol. Macromol.* **24**, 127–138 (1999).

42. Oliveira·, J. M., Pina, S., Reis·, R. L., San, J. & Roman, J. S. *Osteochondral Tissue Engineering*. **1058**, (Springer International Publishing, 2018).

43. Wilson, D., Valluzzi, R. & Kaplan, D. Conformational transitions in model silk peptides. *Biophys. J.* **78**, 2690–2701 (2000).

44. Le Pevelen, D. D. & Tranter, G. E. FT-IR and Raman Spectroscopies, Polymorphism Applications. in *Encyclopedia of Spectroscopy and Spectrometry* 750–761 (Elsevier, 2017). doi:10.1016/B978-0-12-409547-2.12161-4

45. He, S. J., Valluzzi, R. & Gido, S. P. Silk I structure in *Bombyx mori* silk foams. *Int. J. Biol. Macromol.* **24**, 187–195 (1999).

46. Zhang, X. & Pan, Z. Microstructure transitions and dry-wet spinnability of silk fibroin protein from waste silk quilt. *Polymers (Basel).* **11**, 1622 (2019).

47. Motta, A., Fambri, L. & Migliaresi, C. Regenerated silk fibroin films: Thermal and dynamic mechanical analysis. *Macromol. Chem. Phys.* **203**, 1658–1665 (2002).

48. Valluzzi, R., Gido, S. P., Muller, W. & Kaplan, D. L. Orientation of silk III at the air-water interface. *Int. J. Biol. Macromol.* **24**, 237–242 (1999).

49. Akai, H., Nagashima, T. & Aoyagi, S. Ultrastructure of posterior silk gland cells and liquid silk in Indian tasar silkworm, *Antheraea mylitta drury* (Lepidoptera : Saturniidae). *Int. J. Insect Morphol. Embryol.* **22**, 497–506 (1993).

50. Poza, P., Pérez-Rigueiro, J., Elices, M. & LLorca, J. Fractographic analysis of silkworm and spider silk. *Eng. Fract. Mech.* **69**, 1035–1048 (2002).

51. Ebrahimi, D. *et al.* Silk - Its mysteries, how it is made, and how it is used. *ACS Biomater. Sci. Eng.* **1**, 864–876 (2015).

52. Ajisawa, A. Dissolution aqueous of silk fibroin with calciumchloride / ethanol solution. *J. Sericultural Sci. Japan* **67**, 91–94 (1997).

53. Bhat, N. V. & Ahirrao, S. M. Investigation of the structure of silk film regenerated

with lithium thiocyanate solution. *J. Polym. Sci. Polym. Chem. Ed.* **21**, 1273–1280 (1983).

54. Goujon, N., Wang, X., Rajkowa, R. & Byrne, N. Regenerated silk fibroin using protic ionic liquids solvents: Towards an all-ionic-liquid process for producing silk with tunable properties. *Chem. Commun.* **48**, 1278–1280 (2012).

55. Zainuddin *et al.* The behavior of aged regenerated Bombyx mori silk fibroin solutions studied by 1H NMR and rheology. *Biomaterials* **29**, 4268–4274 (2008).

56. Ghosh, S., Parker, S. T., Wang, X., Kaplan, D. L. & Lewis, J. A. Direct-write assembly of microperiodic silk fibroin scaffolds for tissue engineering applications. *Adv. Funct. Mater.* **18**, 1883–1889 (2008).

57. Wang, X., Kluge, J. A., Leisk, G. G. & Kaplan, D. L. Sonication-induced gelation of silk fibroin for cell encapsulation. *Biomaterials* **29**, 1054–1064 (2008).

58. Keten, S., Xu, Z., Ihle, B. & Buehler, M. J. Nanoconfinement controls stiffness, strength and mechanical toughness of β-sheet crystals in silk. *Nat. Mater.* **9**, 359–367 (2010).

59. Knight, D. P. & Vollrath, F. Liquid crystalline spinning of spider silk. *Nature* **410**, 541–548 (2001).

60. Giesa, T., Arslan, M., Pugno, N. M. & Buehler, M. J. Nanoconfinement of spider silk fibrils begets superior strength, extensibility, and toughness. *Nano Lett.* **11**, 5038–5046 (2011).

61. Du, N., Yang, Z., Liu, X. Y., Li, Y. & Xu, H. Y. Structural origin of the strain-hardening of spider silk. *Adv. Funct. Mater.* **21**, 772–778 (2011).

62. Rajkhowa, R., Gupta, V. B. & Kothari, V. K. Tensile stress-strain and recovery behavior of Indian silk fibers and their structural dependence. *J. Appl. Polym. Sci.* **77**, 2418–2429 (2000).

63. Rajkhowa, R. *et al.* Structure and properties of biomedical films prepared from aqueous and acidic silk fibroin solutions. *J. Biomed. Mater. Res. - Part A* **97 A**, 37–45 (2011).

64. Altman, G. H. *et al.* Silk matrix for tissue engineered anterior cruciate ligaments. *Biomaterials* **23**, 4131–4141 (2002).

65. Gellynck, K. *et al.* Silkworm and spider silk scaffolds for chondrocyte support. *J. Mater. Sci. Mater. Med.* **19**, 3399–3409 (2008).

66. Hu, Y., Zhang, Q., You, R., Wang, L. & Li, M. The relationship between secondary structure and biodegradation behavior of silk fibroin scaffolds. *Adv. Mater. Sci. Eng.* **2012**, 1–5 (2012).

67. Wang, Y. *et al.* In vivo degradation of 3D silk fibroin scaffolds. *Biomaterials* **29**, 3415–3428 (2011).

68. Sengupta, S. *et al.* Quantifying osteogenic cell degradation of silk biomaterials. *Biomacromolecules* **11**, 3592–3599 (2010).

69. Daley, W. P., Peters, S. B. & Larsen, M. Extracellular matrix dynamics in development and regenerative medicine. *J. Cell Sci.* **121**, 255–264 (2008).

70. Gomez-Guillen, M. C., Gimenez, B., Lopez-Caballero, M. E. & Montero, M. P. Functional and bioactive properties of collagen and gelatin from alternative sources: A review. *Food Hydrocoll.* **25**, 1813–1827 (2011).

71. Karim, A. A. & Bhat, R. Fish gelatin: properties, challenges, and prospects as an alternative to mammalian gelatins. *Food Hydrocoll.* **23**, 563–576 (2009).

72. P, A. *Thickening and Gelling Agents for Food*. *Thickening and Gelling Agents for Food* (Springer US, 1997). doi:10.1007/978-1-4615-2197-6

73. Eysturskard, J., Haug, I. J., Ulset, A. S. & Draget, K. I. Mechanical properties of mammalian and fish gelatins based on their weight average molecular weight and molecular weight distribution. *Food Hydrocoll.* **23**, 2315–2321 (2009).

74. Davidenko, N. *et al.* Evaluation of cell binding to collagen and gelatin: a study of the effect of 2D and 3D architecture and surface chemistry. *J. Mater. Sci. Mater. Med.* **27**, 148 (2016).

75. Chiou, B. Sen *et al.* Cold water fish gelatin films: Effects of cross-linking on thermal, mechanical, barrier, and biodegradation properties. *Eur. Polym. J.* **44**, 3748–3753 (2008).

76. Panwar, A. & Tan, L. Current status of bioinks for micro-extrusion-based 3D bioprinting. *Molecules* **21**, 685 (2016).

77. Hospodiuk, M., Dey, M., Sosnoski, D. & Ozbolat, I. T. The bioink: A

comprehensive review on bioprintable materials. *Biotechnol. Adv.* **35**, 217–239 (2017).

78. Dash, R., Foston, M. & Ragauskas, A. J. Improving the mechanical and thermal properties of gelatin hydrogels cross-linked by cellulose nanowhiskers. *Carbohydr. Polym.* **91**, 638–645 (2013).

79. Xing, Q. *et al.* Increasing mechanical strength of gelatin hydrogels by divalent metal ion removal. *Sci. Rep.* **4**, 1–10 (2014).

80. Singh, Y. P., Bandyopadhyay, A. & Mandal, B. B. 3D bioprinting using cross-linker-free silk–gelatin bioink for cartilage tissue engineering. *ACS Appl. Mater. Interfaces* **11**, 33684–33696 (2019).

81. Tanaka, A., Nagate, T. & Matsuda, H. Acceleration of wound healing by gelatin film dressings with epidermal growth factor. *J. Vet. Med. Sci.* **67**, 909–913 (2005).

82. Ito, A. *et al.* Transglutaminase-mediated gelatin matrices incorporating cell adhesion factors as a biomaterial for tissue engineering. *J. Biosci. Bioeng.* **95**, 196–199 (2003).

83. Tabata, Y. & Ikada, Y. Protein release from gelatin matrices. *Adv. Drug Deliv. Rev.* **31**, 287–301 (1998).

84. Huang, S. & Fu, X. Naturally derived materials-based cell and drug delivery systems in skin regeneration. *J. Control. Release* **142**, 149–159 (2010).

85. Tabata, Y., Hijikata, S. & Ikada, Y. Enhanced vascularization and tissue granulation by basic fibroblast growth factor impregnated in gelatin hydrogels. *J. Control. Release* **31**, 189–199 (1994).

86. Burdick, J. A. & Anseth, K. S. Photoencapsulation of osteoblasts in injectable RGD-modified PEG hydrogels for bone tissue engineering. *Biomaterials* **23**, 4315–4323 (2002).

87. Nuttelman, C. R., Mortisen, D. J., Henry, S. M. & Anseth, K. S. Attachment of fibronectin to poly(vinyl alcohol) hydrogels promotes NIH3T3 cell adhesion, proliferation, and migration. *J. Biomed. Mater. Res.* **57**, 217–223 (2001).

88. Lee, K. Y., Peters, M. C., Anderson, K. W. & Mooney, D. J. Controlled growth factor release from synthetic extracellular matrices. *Nature* **408**, 998–1000 (2000).

89. Zhang, C. *et al.* Oligo(trimethylene carbonate)-poly(ethylene glycol)-oligo(trimethylene carbonate) triblock-based hydrogels for cartilage tissue engineering. *Acta Biomater.* **7**, 3362–3369 (2011).

90. Varghese, S. & Elisseeff, J. H. Hydrogels for musculoskeletal tissue engineering. *Adv. Polym. Sci.* **203**, 95–144 (2006).

91. Park, H. *et al.* Effect of swelling ratio of injectable hydrogel composites on chondrogenic differentiation of encapsulated rabbit marrow mesenchymal stem cells in vitro. *Biomacromolecules* **10**, 541–546 (2009).

92. Voorhaar, L. & Hoogenboom, R. Supramolecular polymer networks: Hydrogels and bulk materials. *Chem. Soc. Rev.* **45**, 4013–4031 (2016).

93. Hu, W., Wang, Z., Xiao, Y., Zhang, S. & Wang, J. Advances in crosslinking strategies of biomedical hydrogels. *Biomater. Sci.* **7**, 843–855 (2019).

94. Berger, J., Reist, M., Mayer, J. M., Felt, O. & Gurny, R. Structure and interactions in chitosan hydrogels formed by complexation or aggregation for biomedical applications. *Eur. J. Pharm. Biopharm.* **57**, 35–52 (2004).

95. Lehn, J. -M. Supramolecular chemistry - Scope and perspectives molecules, supermolecules, and molecular devices. *Angew. Chemie Int. Ed. English* **27**, 89–112 (1988).

96. Rodell, C. B., Mealy, J. E. & Burdick, J. A. Supramolecular guest-host interactions for the preparation of biomedical materials. *Bioconjug. Chem.* **26**, 2279–2289 (2015).

97. Kakuta, T. *et al.* Preorganized hydrogel: Self-healing properties of supramolecular hydrogels formed by polymerization of host-guest-monomers that contain cyclodextrins and hydrophobic guest groups. *Adv. Mater.* **25**, 2849–2853 (2013).

98. Rüdiger, V. *et al.* Conformational, calorimetric and NMR spectroscopic studies on inclusion complexes of cyclodextrins with substituted phenyl and adamantane derivatives. *J. Chem. Soc., Perkin Trans. 2* **53**, 2119–2123 (1996).

99. Harries, D., Rau, D. C. & Parsegian, V. A. Solutes probe hydration in specific association of cyclodextrin and adamantane. *J. Am. Chem. Soc.* **127**, 2184–2190 (2005).

100. Rodell, C. B., Kaminski, A. L. & Burdick, J. A. Rational design of network properties in guest-host assembled and shear-thinning hyaluronic acid hydrogels. *Biomacromolecules* **14**, 4125–4134 (2013).

101. Wang, L. L. *et al.* Injectable, guest-host assembled polyethylenimine hydrogel for siRNA delivery. *Biomacromolecules* **18**, 77–86 (2017).

102. van de Manakker, F., Vermonden, T., el Morabit, N., van Nostrum, C. F. & Hennink, W. E. Rheological behavior of self-assembling PEG-β-cyclodextrin/PEG-cholesterol hydrogels. *Langmuir* **24**, 12559–12567 (2008).

103. Van Manakker, F. De *et al.* Protein-release behavior of self-assembled PEG-ß-cyclodextrin/PEG- cholesterol hydrogels. *Adv. Funct. Mater.* **19**, 2992–3001 (2009).

104. Charlot, A., Auzély-Velty, R. & Rinaudo, M. Specific interactions in model charged polysaccharide systems. *J. Phys. Chem. B* **107**, 8248–8254 (2003).

105. Chariot, A. & Auzély-Velty, R. Synthesis of novel supramolecular assemblies based on hyaluronic acid derivatives bearing bivalent β-cyclodextrin and adamantane moieties. *Macromolecules* **40**, 1147–1158 (2007).

106. Szejtli, J. Introduction and general overview of cyclodextrin chemistry. *Chem. Rev.* **98**, 1743–1753 (1998).

107. Lagona, J., Mukhopadhyay, P., Chakrabarti, S. & Isaacs, L. The cucurbit[n]uril family. *Angew. Chemie - Int. Ed.* **44**, 4844–4870 (2005).

108. Liu, Y., Guo, D. S., Zhang, H. Y., Ma, Y. H. & Yang, E. C. The structure and thermodynamics of calix[n]arene complexes with dipyridines and phenanthroline in aqueous solution studied by microcalorimetry and NMR spectroscopy. *J. Phys. Chem. B* **110**, 3428–3434 (2006).

109. Sathiyajith, C. W. *et al.* Biological and related applications of pillar[n]arenes. *Chem. Commun.* **53**, 677–696 (2017).

110. Nikitenko, N. A. & Prassolov, V. S. Non-viral delivery and therapeutic application of small interfering RNAs. *Acta Naturae* **5**, 35–53 (2013).

111. Ahmed, M. S. *et al.* A supramolecular nanocarrier for delivery of amiodarone anti-arrhythmic therapy to the heart. *Bioconjug. Chem.* **30**, 733–740 (2019).

112. Biwer, A., Antranikian, G. & Heinzle, E. Enzymatic production of cyclodextrins. *Appl. Microbiol. Biotechnol.* **59**, 609–617 (2002).

113. Guvendiren, M., Lu, H. D. & Burdick, J. A. Shear-thinning hydrogels for biomedical applications. *Soft Matter* **8**, 260–272 (2012).

114. Patenaude, M., Smeets, N. M. B. & Hoare, T. Designing injectable, covalently cross-linked hydrogels for biomedical applications. *Macromol. Rapid Commun.* **35**, 598–617 (2014).

115. Censi, R., Fieten, P. J., Di Martino, P., Hennink, W. E. & Vermonden, T. *In-situ* forming hydrogels by simultaneous thermal gelling and Michael addition reaction between methacrylate bearing thermosensitive triblock copolymers and thiolated hyaluronan. *J. Control. Release* **148**, e28–e29 (2010).

116. Goodarzi, H., Jadidi, K., Pourmotabed, S., Sharifi, E. & Aghamollaei, H. Preparation and in vitro characterization of cross-linked collagen–gelatin hydrogel using EDC/NHS for corneal tissue engineering applications. *Int. J. Biol. Macromol.* **126**, 620–632 (2019).

117. Skardal, A. *et al.* Photocrosslinkable hyaluronan-gelatin hydrogels for two-step bioprinting. *Tissue Eng. - Part A* **16**, 2675–2685 (2010).

118. Cohen, D. L., Malone, E., Lipson, H. & Bonassar, L. J. Direct freeform fabrication of seeded hydrogels in arbitrary geometries. *Tissue Eng.* **12**, 1325–1335 (2006).

119. Ouyang, L., Highley, C. B., Rodell, C. B., Sun, W. & Burdick, J. A. 3D printing of shear-thinning hyaluronic acid hydrogels with secondary cross-linking. *ACS Biomater. Sci. Eng.* **2**, 1743–1751 (2016).

120. Moreira Teixeira, L. S., Feijen, J., van Blitterswijk, C. A., Dijkstra, P. J. & Karperien, M. Enzyme-catalyzed crosslinkable hydrogels: Emerging strategies for tissue engineering. *Biomaterials* **33**, 1281–1290 (2012).

121. Hu, J. *et al.* Visible light crosslinkable chitosan hydrogels for tissue engineering. *Acta Biomater.* **8**, 1730–1738 (2012).

122. Cidonio, G., Glinka, M., Dawson, J. I. & Oreffo, R. O. C. The cell in the ink: Improving biofabrication by printing stem cells for skeletal regenerative medicine. *Biomaterials* **209**, 10–24 (2019).

123. Wu, Z. *et al.* Bioprinting three-dimensional cell-laden tissue constructs with controllable degradation. *Sci. Rep.* **6**, 1–10 (2016).

124. Ozbolat, I. T. Scaffold-based or scaffold-free bioprinting: Competing or complementing approaches? *J. Nanotechnol. Eng. Med.* **6**, 1–6 (2015).

125. Das, S. *et al.* Decellularized extracellular matrix bioinks and the external stimuli to enhance cardiac tissue development in vitro. *Acta Biomater.* **95**, 188–200 (2019).

126. Levato, R. *et al.* Biofabrication of tissue constructs by 3D bioprinting of cell-laden microcarriers. *Biofabrication* **6**, 035020 (2014).

127. Norotte, C., Marga, F. S., Niklason, L. E. & Forgacs, G. Scaffold-free vascular tissue engineering using bioprinting. *Biomaterials* **30**, 5910–5917 (2009).

128. Jakab, K. *et al.* Tissue engineering by self-assembly and bio-printing of living cells. *Biofabrication* **2**, 022001 (2010).

129. Melchels, F. P. W. *et al.* Additive manufacturing of tissues and organs. *Prog. Polym. Sci.* **37**, 1079–1104 (2012).

130. Hollister, S. J. Porous scaffold design for tissue engineering. *Nat. Mater.* **4**, 518–524 (2005).

131. Ballyns, J. J. & Bonassar, L. J. Image-guided tissue engineering. *J. Cell. Mol. Med.* **13**, 1428–1436 (2009).

132. Paolini, A., Kollmannsberger, S. & Rank, E. Additive manufacturing in construction: A review on processes, applications, and digital planning methods. *Addit. Manuf.* **30**, 100894 (2019).

133. Wilson, W. C. & Boland, T. Cell and organ printing 1: Protein and cell printers. *Anat. Rec. - Part A Discov. Mol. Cell. Evol. Biol.* **272**, 491–496 (2003).

134. Fedorovich, N. E., De Wijn, J. R., Verbout, A. J., Alblas, J. & Dhert, W. J. A. Three-dimensional fiber deposition of cell-laden, viable, patterned constructs for bone tissue printing. *Tissue Eng. - Part A.* **14**, 127–133 (2008).

135. Li, S. *et al.* Gradient hydrogel construct based on an improved cell assembling system. *J. Bioact. Compat. Polym.* **24**, 84–99 (2009).

136. Derby, B. Bioprinting: Inkjet printing proteins and hybrid cell-containing materials

and structures. *J. Mater. Chem.* **18**, 5717–5721 (2008).

137. Hölzl, K. *et al.* Bioink properties before, during and after 3D bioprinting. *Biofabrication* **8**, 1–19 (2016).

138. Guillotin, B. *et al.* Laser assisted bioprinting of engineered tissue with high cell density and microscale organization. *Biomaterials* **31**, 7250–7256 (2010).

139. Murphy, S. V. & Atala, A. 3D bioprinting of tissues and organs. *Nat. Biotechnol.* **32**, 773–785 (2014).

140. Chang, R., Nam, J. & Sun, W. Effects of dispensing pressure and nozzle diameter on cell survival from solid freeform fabrication-based direct cell writing. *Tissue Eng. - Part A.* **14**, 41–48 (2008).

141. Tubío, C. R., Guitián, F. & Gil, A. Fabrication of ZnO periodic structures by 3D printing. *J. Eur. Ceram. Soc.* **36**, 3409–3415 (2016).

142. Torres, M. D. Role of the rheology in the new emerging technologies as 3D printing. *Rheol. Open Access* **1**, 3–4 (2017).

143. Wang, L., Zhang, M., Bhandari, B. & Yang, C. Investigation on fish surimi gel as promising food material for 3D printing. *J. Food Eng.* **220**, 101–108 (2018).

144. Sasaki, N. Viscoelastic properties of biological materials. in *Viscoelasticity - From Theory to Biological Applications* **i**, 13 (InTech, 2012).

145. Malvern Instruments. Understanding yield stress measurements. *Annu. Trans. Nord. Rheol. Soc.* **21**, 6 (2012).

146. Uchikawa, H. Handbook of analytical techniques in concrete science and technology. in *Handbook of Analytical Techniques in Concrete Science and Technology* 820–934 (2001). doi:10.1016/B978-081551437-4.50023-0

147. Schuurman, W. *et al.* Gelatin-methacrylamide hydrogels as potential biomaterials for fabrication of tissue-engineered cartilage constructs. *Macromol. Biosci.* **13**, 551–561 (2013).

148. Aguado, B. A., Mulyasasmita, W., Su, J., Lampe, K. J. & Heilshorn, S. C. Improving viability of stem cells during syringe needle flow through the design of hydrogel cell carriers. *Tissue Eng. - Part A* **18**, 806–815 (2012).

149. Buckwalter, J. A., Saltzman, C. & Brown, T. The impact of osteoarthritis. *Clin.*

Orthop. Relat. Res. **427**, S6–S15 (2004).

150. Macario, D. K., Entersz, I., Paul Abboud, J. & Nackman, G. B. Inhibition of apoptosis prevents shear-induced detachment of endothelial cells. *J. Surg. Res.* **147**, 282–289 (2008).

151. Saunders, R. E., Gough, J. E. & Derby, B. Delivery of human fibroblast cells by piezoelectric drop-on-demand inkjet printing. *Biomaterials* **29**, 193–203 (2008).

152. Khalil, S. & Sun, W. Bioprinting endothelial cells with alginate for 3D tissue constructs. *J. Biomech. Eng.* **131**, 1–8 (2009).

153. Fedorovich, N. E. *et al.* Biofabrication of osteochondral tissue equivalents by printing topologically defined, cell-laden hydrogel scaffolds. *Tissue Eng. - Part C Methods* **18**, 33–44 (2012).

154. Rezende, R. A., Bártolo, P. J., Mendes, A. & Filho, R. M. Rheological behavior of alginate solutions for biomanufacturing. *J. Appl. Polym. Sci.* **113**, 3866–3871 (2009).

155. Bajaj, P., Schweller, R. M., Khademhosseini, A., West, J. L. & Bashir, R. 3D biofabrication strategies for tissue engineering and regenerative medicine. *Annu. Rev. Biomed. Eng.* **16**, 247–276 (2014).

156. Guillemot, F., Mironov, V. & Nakamura, M. Bioprinting is coming of age: Report from the international conference on bioprinting and biofabrication in Bordeaux (3B'09). in *Biofabrication* **2**, (2010).

157. Das, S. *et al.* Bioprintable, cell-laden silk fibroin-gelatin hydrogel supporting multilineage differentiation of stem cells for fabrication of three-dimensional tissue constructs. *Acta Biomater.* **11**, 233–246 (2015).

158. Gungor-Ozkerim, P. S., Inci, I., Zhang, Y. S., Khademhosseini, A. & Dokmeci, M. R. Bioinks for 3D bioprinting: An overview. *Biomater. Sci.* **6**, 915–946 (2018).

159. Das, S. *et al.* Enhanced redifferentiation of chondrocytes on microperiodic silk/gelatin scaffolds: Toward tailor-made tissue engineering. *Biomacromolecules* **14**, 311–321 (2013).

160. Shanmugam, M. *et al.* Host-guest interaction of l-tyrosine with β-cyclodextrin. *Spectrochim. Acta - Part A Mol. Biomol. Spectrosc.* **71**, 125–132 (2008).

161. Hafidz, R. N. R. M., Yaakob, C. M., Amin, I. & Noorfaizan, A. Chemical and functional properties of bovine and porcine skin gelatin. *Int. Food Res. J.* **18**, 787–791 (2011).

162. Hong, B. M., Park, S. A. & Park, W. H. Effect of photoinitiator on chain degradation of hyaluronic acid. *Biomater. Res.* **23**, 21 (2019).

163. Zhang, X. M., Peng, C. S. & Xu, G. C. Synthesis of modified β-cyclodextrin polymers and characterization of their fuchsin adsorption. *J. Incl. Phenom. Macrocycl. Chem.* **72**, 165–171 (2012).

164. Habeeb, A. F. S. A. Determination of free amino groups in proteins by trinitrobenzenesulfonic acid. *Anal. Biochem.* **14**, 328–336 (1966).

165. Claaßen, C. *et al.* Quantification of substitution of gelatin methacryloyl: Best practice and current pitfalls. *Biomacromolecules* **19**, 42–52 (2018).

166. Karvinen, J., Ihalainen, T. O., Calejo, M. T., Jönkkäri, I. & Kellomäki, M. Characterization of the microstructure of hydrazone crosslinked polysaccharide-based hydrogels through rheological and diffusion studies. *Mater. Sci. Eng. C* **94**, 1056–1066 (2019).

167. Piskounova, S., Rojas, R., Bergman, K. & Hilborn, J. The effect of mixing on the mechanical properties of hyaluronan-based injectable hydrogels. *Macromol. Mater. Eng.* **296**, 944–951 (2011).

168. Crumling, M. A., King, K. A. & Duncan, R. K. Cyclodextrins and iatrogenic hearing loss: New drugs with significant risk. *Frontiers in Cellular Neuroscience* **11**, 355 (2017).

169. Sigma-Aldrich. Succinyl-β-cyclodextrin. Available at: https://www.sigmaaldrich.com/catalog/product/sigma/85990?lang=pt&region=PT. (Accessed: 5th April 2020)

170. Fisher, T. EDC (1-ethyl-3-(3-dimethylaminopropyl)carbodiimide hydrochloride). Available at: https://www.thermofisher.com/order/catalog/product/22980#/22980. (Accessed: 5th April 2020)

171. Perng, J. K. *et al.* Ultrasound imaging of oxidative stress in vivo with chemically-generated gas microbubbles. *Ann. Biomed. Eng.* **40**, 2059–2068 (2012).

172. Manuscript, A. Effect of silk protein processing on drug delivery from silk films. **13**, 617–627 (2014).

173. Knowlton, S., Yenilmez, B., Anand, S. & Tasoglu, S. Photocrosslinking-based bioprinting: Examining crosslinking schemes. *Bioprinting* **5**, 10–18 (2017).

174. Heo, J. *et al.* Riboflavin-induced photo-crosslinking of collagen hydrogel and its application in meniscus tissue engineering. *Drug Deliv. Transl. Res.* **6**, 148–158 (2016).

175. Navarro, J., Swayambunathan, J., Lerman, M., Santoro, M. & Fisher, J. P. Development of keratin-based membranes for potential use in skin repair. *Acta Biomater.* **83**, 177–188 (2019).

176. Cardoso, D. R., Libardi, S. H. & Skibsted, L. H. Riboflavin as a photosensitizer. Effects on human health and food quality. *Food Funct.* **3**, 487 (2012).

177. Kwaambwa, H. M., Goodwin, J. W., Hughes, R. W. & Reynolds, P. A. Viscosity, molecular weight and concentration relationships at 298 K of low molecular weight cis-polyisoprene in a good solvent. *Colloids Surfaces A Physicochem. Eng. Asp.* **294**, 14–19 (2007).

178. Perera, D. *et al.* The effect of polymer molecular weight and cell seeding density on viability of cells entrapped within PEGDA hydrogel microspheres. *J. Microencapsul.* **35**, 475–481 (2018).

179. Lee, B. H., Li, B. & Guelcher, S. A. Gel microstructure regulates proliferation and differentiation of MC3T3-E1 cells encapsulated in alginate beads. *Acta Biomater.* **8**, 1693–1702 (2012).

180. Caliari, S. R. & Burdick, J. A. A practical guide to hydrogels for cell culture. *Nat. Methods* **13**, 405–414 (2016).

181. Sigma-Aldrich. Product information - Gelatin. Available at: https://www.sigmaaldrich.com/content/dam/sigma-aldrich/docs/Sigma/Product_Information_Sheet/2/g9382pis.pdf. (Accessed: 4th May 2020)

182. Instruments, T. Thermal solutions - Determination of the linear viscoelastic region of a polymer using a strain sweep on the DMA 2980. Available at: http://www.tainstruments.com/pdf/literature/TS61.pdf. (Accessed: 6th May 2020)

183. Cuomo, F., Cofelice, M. & Lopez, F. Rheological characterization of hydrogels from alginate-based nanodispersion. *Polymers (Basel).* **11**, 259 (2019).

184. Mezger, T. G. *The Rheology Handbook*. (European Coatings Library, 2004).